Applied Energy

Optimal Dynamic Dispatch for AC Microgrids with Power Factor Correction under Supply and Demand Uncertainty

--Manuscript Draft--

Manuscript Number:	APEN-D-24-02606
Article Type:	VSI: Microgrids 2025(Chris Marnay)
Keywords:	Microgrids; Energy Systems; Optimization; Grid Stability; Rolling Horizon; Pareto Front
Abstract:	This study presents an Optimal Dynamic Dispatch (ODD) framework utilizing mixed-integer linear programming (MILP) to coordinate distributed energy resources while considering power factor (PF) for operational efficiency. In general, unit commitment models commonly overlook the influence of power quality on transmission power losses and the potential impact of demand-side management (DSM) on grid stability when faced with uncertain supply and demand conditions. Our framework addresses these issues by incorporating an MILP that accounts for both PF and DSM, employs an -constraint method for multi-objective optimization, and utilizes a rolling horizon heuristic for computational efficiency. Applied to the IEEE 18-bus and IEEE 30-bus systems, the ODD framework identifies an optimal PF of 0.95 for voltage control, resulting in a 10% reduction in active demand and a substantial 60% reduction in reactive demand. Furthermore, utilizing the -constraint approach results in a notable decrease of carbon emissions (CO2) by as much as 66% in the IEEE 18-bus system, accompanied by a moderate cost increase of 19%. Similarly, applying this method in the IEEE 30-bus systems reduces CO2 emissions by up to 50% while incurring a cost increase of 12%. The rolling horizon heuristic significantly improves computational efficiency by breaking down the original problem into manageable sub-problems, offering a promising approach for real-time decision-making in energy systems.

UNIVERSITY
OF MIAMI

Dept. of Industrial and Systems Engineering
University of Miami

1251 Memorial Drive
McArthur Engr. Bldg., Room 280
Coral Gables, FL 33146

February 21, 2024

Guest Editors, Virtual Special Issue on Microgrids

Prof. Chris Marnay, Lawrence Berkeley Nat. Lab., U.S.A.
Prof. Tao Xu, Tianjin University, China
Prof. Nikos Hatziargyriou, Nat. Tech. University of Athens, Greece
Prof. Yuko Hirase, Toyo University, Japan
Prof. Patricio Mendoza-Araya, University of Chile
Prof. Shuai Lu, Southeast University, China

Dear Guest Editors,

Enclosed, please find one original of the manuscript entitled, "Optimal Dynamic Dispatch for AC Microgrids with Power Factor Correction under Supply and Demand Uncertainty", by Abdullah Alsaheal, Joshua Darville, Haluk Damgacioglu, Murat Erkoc, and myself to be considered for publication in Applied Energy & Advances in Applied Energy: Special Issue on Microgrids 2025. This paper contributes a method to the literature that addresses the commonly overlooked influence of power quality on transmission power losses and the potential impact of demand-side management on grid stability, significantly enhancing computational efficiency and offering a promising approach for real-time decision-making in energy systems. It could potentially help catalyze commercial adoption of modeling in microgrid operations.

The manuscript submitted is a full-length article with 10,678 words (excluding the Abstract and Keywords, and including References), 9 figures and 6 tables, and has neither been submitted elsewhere nor has it appeared in print. All communications concerning the paper may be sent to the above address.

Thank you for your attention, and we are looking forward to hearing from you.

Yours truly,

Nurcin Celik

Nurcin Celik, Ph.D.
Professor
Department of Industrial and Systems Engineering
Director, Simulation and Optimization Research Laboratory
Faculty Advisor, Society of Women Engineers
University of Miami

Highlights

1. Decision-making framework for autonomous microgrid (MG) control under uncertainty
2. AC-MG policy coordinating DERs, power flow, power factor, frequency, and DSM
3. Hybrid rolling horizon heuristic with ϵ-constraint method to solve AC-MG policy
4. Hybrid approach obtains a feasible solution and improves computational efficiency
5. Faults are addressed in sequence using renewables, non-renewables and finally DSM

Optimal Dynamic Dispatch for AC Microgrids with Power Factor Correction under Supply and Demand Uncertainty

Abdullah Alsaheal
University of Miami
1251Memorial Dr.
McArthur Engineering Building, Room 287
Coral Gables, FL 33146, USA
a.alsaheal@miami.edu

Joshua Darville
University of Miami
1251Memorial Dr.
McArthur Engineering Building, Room 157
Coral Gables, FL 33146, USA
jmd437@miami.edu

Haluk Damgacioglu
University of Texas
1200 Pressler Street
School of Public Health
Houston, TX 77030 USA
haluk.damgacioglu@uth.tmc.edu

Nurcin Celik*
University of Miami
1251Memorial Dr.
McArthur Engineering Building, Room 280
Coral Gables, FL 33146, USA
celik@miami.edu

Murat Erkoc
University of Miami
1251Memorial Dr.
McArthur Engineering Building, Room 283
Coral Gables, FL 33146, USA
merkoc@miami.edu

*Corresponding Author

Abstract – This study presents an Optimal Dynamic Dispatch (ODD) framework utilizing mixed-integer linear programming (MILP) to coordinate distributed energy resources while considering power factor (PF) for operational efficiency. In general, unit commitment models commonly overlook the influence of power quality on transmission power losses and the potential impact of demand-side management (DSM) on grid stability when faced with uncertain supply and demand conditions. Our framework addresses these issues by incorporating an MILP that accounts for both PF and DSM, employs an ϵ-constraint method for multi-objective optimization, and utilizes a rolling horizon heuristic for computational efficiency. Applied to the IEEE 18-bus and IEEE 30-bus systems, the ODD framework identifies an optimal PF of 0.95 for voltage control, resulting in a 10% reduction in active demand and a substantial 60% reduction in reactive demand. Furthermore, utilizing the ϵ-constraint approach results in a notable decrease of carbon emissions (CO2) by as much as 66% in the IEEE 18-bus system, accompanied by a moderate cost increase of 19%. Similarly, applying this method in the IEEE 30-bus systems reduces CO2 emissions by up to 50% while incurring a cost increase of 12%. The rolling horizon heuristic significantly improves computational efficiency by breaking down the original problem into manageable sub-problems, offering a promising approach for real-time decision-making in energy systems.

Keywords – Energy Systems; Optimization; Grid Stability; Rolling Horizon; Pareto Front

ABBREVIATIONS

DER	Distributed Energy Resource
MG	Microgrids
SG	Smart Grids
CO_2	Carbon Emissions
UC	Unit Commitment
MILP	Mixed Integer Linear Programming
PF	Power Factor
ODD	Optimal Dynamic Dispatch
AC	Alternating Current
DC	Direct Current
DSM	Demand-Side Management
RF	Rate of Change of Frequency
TSO	Transmission System Operator
PLA	Piecewise Linear Approximation
EV	Electric Vehicles
SOC	State of Charge
SH	Scheduling Horizon
PH	Planning Horizon
CH	Control Horizon

1 INTRODUCTION

Conventional power grids, characterized by hierarchical structures, are susceptible to cascading failures [1], [2], rendering them vulnerable to many disruptions. The transition towards smart grids (SGs) represents a concerted effort to integrate self-healing capabilities and enhance resilience in the face of anomalous events, encompassing demand and supply fluctuations, infrastructure damage, and cyber threats, all orchestrated through the effective coordination of diverse DERs within the existing power grid [3], [4]. Within this context, microgrids (MGs) emerge as self-reliant sub-networks [5]–[7] capable of isolating faults before they propagate throughout the entire grid [8]–[10], thereby significantly enhancing the resilience of SGs. Hence, the efforts to achieve energy resilience present a significant challenge due to increasing energy consumption, the intermittent nature of distributed energy resources (DERs), and the necessity to reduce carbon dioxide (CO2) emissions in generating power. In response to the complex challenges of dynamic dispatch decision-making within MGs, this paper proposes an optimal dynamic dispatch (OOD) framework for scheduling DERs that addresses the challenges of *i*) decreasing the total operating cost for an energy provider (utility) while reducing the environmental impact of MG operations, *ii*) automating decision-making under stochastic supply and demand in a scalable manner, and *iii*) sustaining the overall grid stability during a contingency.

1.1 Problem Statement

The first challenge of MG dispatch is often referred to as the unit commitment (UC) problem. The UC problem is a fundamental short-term, sequential decision-making problem that describes scheduling dispatchable generators in an MG to reduce cost and emissions while reliably balancing supply and demand. Numerous factors make the UC problem challenging, including a high dimensional solution space, using binary variables to select thermal generation units and the physical limitations of DERs for MG operation [11]. Thus, many previous studies used mixed integer linear programming (MILP) to address the challenge of automating decision-making under uncertainty and finding the optimal combination of UC decisions for a MILP's objective [12]–[14]. However, there is a gap in the literature on how to effectively model the

impact of poor power quality on an MG's operating efficiency and stability while considering the logistics of power transfer. While the challenge of sustaining the overall grid stability during a contingency was not considered in the previous studies, this study aims to fill this gap by developing an MG dispatch policy that considers the effect of power factor (PF) on MG efficiency and the impact of demand-side management (DSM) on grid stability. We tackle the UC problem using a convex optimization paradigm that exploits the property of convexity in a high dimensional problem [15], [16] and contribute to the existing literature by introducing an optimal dynamic dispatch (ODD) framework for near real-time decision-making in alternating current (AC) MGs. Within this proposed framework, the MG dispatch policy module i) minimizes both MG operational costs and CO_2 emissions, ii) controls MG operating efficiency, and iii) sustains MG stability and power quality via DSM. Furthermore, we propose a rolling horizon heuristic module to tackle computational complexity and obtain the best compromise solution throughout the overall scheduling horizon by dividing the original problem into smaller sub-problems.

1.2 Literature Review

Various assumptions are necessary when formulating the UC problem as a MILP. For example, the direct current (DC) network representation of the UC problem (DC-UC) considers Kirchhoff's current law and assumes reactive power flow is negligible, phase angles are small, and voltage is constant [12], [13]. While a DC-UC problem is generally tractable, [14] suggests a post-analysis should be conducted to check the results' feasibility. However, the alternating current (AC) network representation of the UC problem (AC-UC) considers Kirchhoff laws with non-linear constraints to capture harmonic power flow behavior throughout the network. We assumed the latter when modeling the UC problem, which provides a comparatively more accurate depiction of MG operations. The AC-UC problem is known as intractable due to the mixed integer variables when modeling the non-linear nature of AC power flow [15]. Therefore, our formulation uses the linearized AC power flow physics equations *(LinDistFlow)* proposed by [16] through the inner approximation method. The *LinDistFlow* equations were also considered by [17] in a variate of the AC-UC problem, which considers network reconfiguration of the transmission lines to enhance MG's reliability in islanded mode. After selecting the type of electrical network to model, a DSM program is used to facilitate a reduction in the market-clearing price of energy during peak hours despite projected increases in demand. Moreover, a DSM program incentivizes consumer participation in energy management across decentralized MGs, assuming that customers are linked via smart metering technology and appliances can be controlled remotely.

The authors [17]–[19] use DSM programs within their MILPs to implement load shedding. However, the latter presents a multi-objective model considering customer satisfaction instead of the environmental cost incurred by CO_2 emissions in the former. The Pareto front for each model was generated in these studies via the ϵ - constraint method [20] and δ - constraint method [21], respectively. Like these previous studies, our DSM program controls loads to satisfy the utility's load-shedding requirements. Here, controllable loads are classified into three groups according to [22], including i) shiftable loads, which may change their working time; ii) dimmable loads, which may modify their power consumption based on the consumer price; and iii) static loads which only have a binary (on/off) state. To minimize the impact on consumers during load shedding, we select the minimum number of controllable loads to regulate within an MG dispatch policy. Moreover, a similar assumption to [23] is made for consumer privacy concerns where consumers have permitted their static loads to be regulated under our proposed DSM program.

Although [19] also implemented a DSM program in their proposed MG formulation, this formulation does not consider the electrical operating frequency required to sustain an MG's stability under various contingencies. Additionally, a study by [24] places significant emphasis on the day-ahead optimal scheduling of a microgrid. Their primary objective is to investigate the effectiveness of DSM control,

energy storage systems, and uncertainty management to enhance operational cost efficiency and mitigate emission pollution. This study focuses on customer clustering to optimize energy consumption while not explicitly considering the electrical operating frequency required to sustain MG stability. Due to its low inertial characteristics, the electrical frequency must remain within operating limits for an MG to function reliably. Thus, large deviations in the energy supply or demand may result in similar deviations in the operating frequency [25]. The rate of change of frequency (RF) is directly influenced by the coordination of various DERs to sustain the MG's stability. Since the swing equation captures the frequency dynamics of an MG according to [26], [27] utilizes the swing equation to model the effect of frequency on the MG's stability and determines the minimal amount of load shedding required to stabilize the MG. Thus, DERs, such as storage units, can act as an aggregated group of fast reactors to readily inject/absorb power from an MG, which makes them ideal for frequency regulation [25] by a transmission system operator (TSO).

Similarly, [28] uses electric vehicles as another class of generators to readily inject/absorb power for frequency regulation. Despite accounting for frequency regulation, these models do not consider the impact of CO2 emissions, which was considered in the previous studies. Another study by [29] focuses on optimizing economic and emission costs. They consider several parameters, including the capacity of electric vehicle (EV) batteries, state of charge (SOC) of these batteries, charge/discharge schedules for EVs, and the percentage of EVs present in a parking lot. Their primary focus is optimizing economic and emission-related factors in microgrid planning without placing much emphasis on near-real-time decision-making or resiliency considerations.

Moreover, the MG's power factor (PF) determines power quality throughout an electric grid. Thus, identifying DERs and transmission lines with a high PF is essential for MG operational efficiency [30]. The effect of active demand mismatch between a utility and its consumers due to power flow harmonics during load shedding was described by [30]. However, the reactive demand mismatch was not considered in [34] and was later addressed by [35]. Since both active and reactive demand mismatch must be resolved to sustain grid stability, both types of demand are considered in the proposed MG dispatch policy. In addition to considering power quality in our MG dispatch policy module, we integrate power flow physics and embed a DSM program to model the AC-UC problem accurately. Our MG dispatch policy module uses convex optimization to solve an MILP that minimizes the operational cost for an MG in grid-connected mode with the main utility grid.

However, the MILP formulations for MG dispatch policies thus far do not present a computationally efficient solution method for larger problem instances except [32] and [33]. The rolling horizon approach is a reactive scheduling technique that solves scheduling problems under uncertainty. Two applications of the rolling horizon technique can be observed in the field of network management using multi-parametric programming [32], as well as in the coordination of DERs inside a microgrid (MG) to maximize profit [33]. Although the rolling horizon approach has been used in [33] and [34], it has not been applied to MG dispatch for the AC-UC problem defined in our study. Therefore, there is a need for an MG dispatch model that coordinates various types of DERs under stochastic supply and demand while sustaining the MG stability with a viable solution method. This study seeks to fill this research gap by using the proposed ODD framework to address the challenges associated with MG dispatch. First, our MG dispatch policy module within the proposed ODD framework considers the diverse challenges of MG dispatch outlined in the previous studies. Second, we use a rolling horizon heuristic to iteratively obtain MG dispatch decisions over a fixed time horizon, providing a scalable solution for larger problem instances and power network expansion. Simultaneously, the ϵ-constraint method resolves conflicting objectives within the MG dispatch policy to select a best-compromise solution for the given planning horizon. The various challenges of MG dispatch outlined in previous studies throughout the literature are compared in **Table 1**.

Table 1: MG dispatch features from the literature

Study	Multi-objective	AC Power Flow	Power Quality	Demand-side Management	Frequency Control
[3], [4], [22]				✓	
[13], [19], [21], [35]	✓			✓	
[25], [26]	✓				✓
[27], [28]				✓	✓
[30]			✓		
[17], [36]		✓	✓		
Proposed Work	✓	✓	✓	✓	✓

1.3 Contributions and Organization

To the best of our knowledge, the proposed MG dispatch policy is the first MILP formulation that simultaneously considers linearized AC power flow physics equations, UC under supply and demand uncertainty, PF correction using DSM, and frequency control. We evaluate the decision-making capabilities of the proposed MG dispatch policy on the IEEE 18-bus and IEEE 30-bus networks. The proposed MG dispatch policy identifies poor-performing DERs and transmission lines with low PF. These DERs and transmission lines may need to be replaced with energy assets with a higher PF or resized to meet the projected future energy demand. Otherwise, additional capacity is integrated via renewables, capacitors, or DSM. The resulting dispatch decisions ensure sustainable voltage levels while limiting line losses during transmission.

Subsequent sections of this manuscript are organized as follows. In Section 2, we define the AC-UC problem structure, propose a mathematical MILP formulation for an MG system, and present a solution technique for both multi-objectivity and computational efficiency. In Section 3, we test our proposed MG dispatch policy on the IEEE 18-bus and IEEE 30-bus networks and discuss the results. Finally, we conclude the findings of this study, provide key insights, and discuss future work in Section 4.

2 MODELING STOCHASTIC AC MICROGRIDS USING MIXED INTEGER LINEAR PROGRAMMING

MILP is used for sequential decision-making under uncertainty and is often referred to as a policy. Here, a policy (π) uses information known at time t to map the system's state to a feasible solution. Thus, we define our stochastic AC-UC problem according to the canonical framework given in (1) and (2) proposed by [37] and [38].

2.1 AC-UC Problem Definition

$$min_{\pi}\, \mathbf{E}^{\pi}\left[\sum_{\omega\in\Omega} P(\omega) \times \sum_{t\in\mathcal{T}} C(S_t, X_t^{\pi}(S_t))|S_0\right] \tag{1}$$

$$st: S_{t+1} = S^{M}(S_t, X_t^{\pi}, (S_t), W_{t+1}(\omega)) \tag{2}$$

The notation used in this canonical framework highlights three major components of any sequential decision-making problem. These components include state variables (S_t), decision variables (X_t), and exogenous information (W_t), which is often subject to uncertainty. A transition function (S^M) describes

how states evolve according to a Markov decision-making process. Moreover, all future events are captured by a sample set (Ω). A sample realization (ω) of this set is described with a scenario tree, where each scenario can have a unique weighting [39]. Furthermore, the time, state, and actions are discretized along a finite planning horizon for day-ahead scheduling to limit the combinatorial expansion associated with MILP for tractability purposes. Thus, we formulate an MG dispatch policy (π) for an MG system using MILP for sequential decision-making and embed it within the proposed ODD framework.

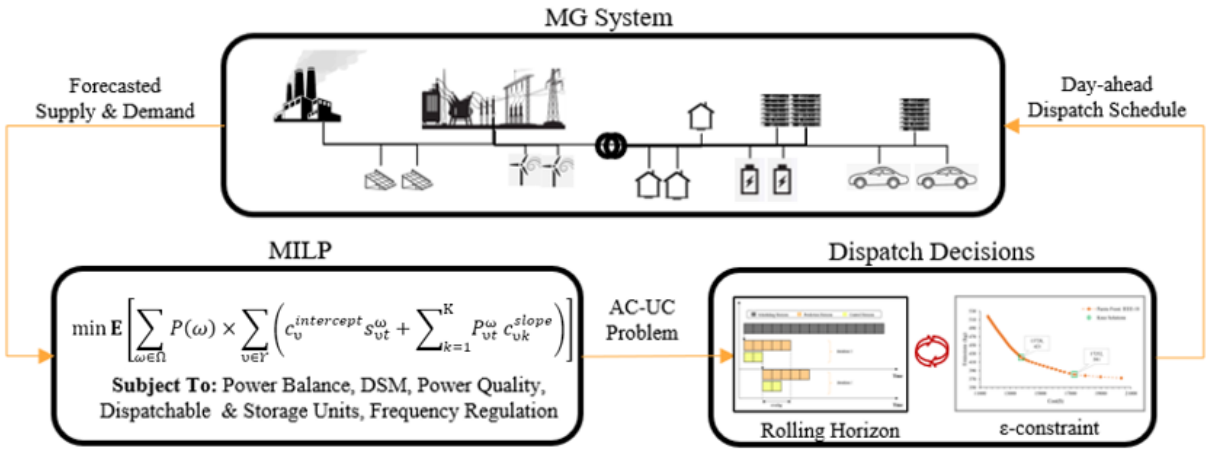

Figure 1. Proposed ODD framework for near real-time decision-making in AC MGs

The ODD framework in **Figure 1** outlines a series of methods used to obtain MG dispatch decisions near real-time. First, a centralized energy provider (utility) is coupled to the MG system, which readily exchanges power with local consumer markets based on forecasted supply and demand. Second, the utility uses a MILP formulation of the AC-UC problem to obtain the optimal dispatch decision for a given scenario. A DSM program is embedded within the MG dispatch policy and incentivizes consumers to allow the utility to regulate consumer static loads. This regulation allows the utility to reduce peak demand, subsequently reducing the market-clearing price of energy [40], [41] while sustaining the MG's stability. The goal of the proposed MG dispatch policy is to reduce the cost of energy production while considering the conflicting amount of CO_2 emissions required to produce energy. Finally, the MILP formulation coordinates various DERs for day-ahead scheduling. Due to the size and complexity of the AC-UC problem under stochastic conditions, the AC-UC problem is often infeasible to solve in a timely manner. To address the challenges of MG dispatch outlined in **Table 1** over a long-time horizon, a rolling horizon heuristic is employed to iteratively obtain MG dispatch decisions over smaller periods throughout the entire time horizon. Subsequently, these solutions are scrutinized using the ϵ-constraint method to select the best compromise solution from a set of MG dispatch decisions for a given scenario.

The MG dispatch policy assumes that i) smart metering technology has enabled consumer markets to anticipate peak hours and incentivizes a cooperative response, ii) the main utility provider has an existing DSM program to regulate consumer demand, iii) renewable generation is regulated using storage units a day ahead of production, and iv) only positive sequence components [40], [41] exist in a balanced three-phase AC MG system. If assumption iv is violated, it implies the presence of negative sequence components in the system, causing the network to operate under unbalanced conditions [42], which is not considered in this study. Sources of uncertainty considered in the MG dispatch policy are derived from exogenous variables such as internal consumer demand and external climate factors. These external climate factors include solar irradiance, ambient temperature, and wind speed and are modeled by (3)-(16) in [43].

Exogenous information becomes known at time t including the net forecasted demand, renewable power injections, and cross-border power exchange. The nomenclature used to model the proposed MG dispatch policy is outlined in **Tables 2a and 2b**.

Table 2a: Nomenclature for proposed MG dispatch policy

Sets	
$\mathcal{N}\{i\}$	Neighborhood of node i
$\mathcal{N}$	Set of nodes (buses), $\mathcal{N} = \{1, \dots, i, \dots, \mathcal{N}\}$
$\mathrm{Z}\{i\}$	Set of appliances, $\mathrm{Z} = \{1, \dots, \zeta, \dots, Z\}$
$\mathcal{T}$	Set of time periods, $\mathcal{T} = \{1, \dots, t, \dots, \mathcal{T}\}$
$\mathcal{E}$	Set of edges, $(i, j) \in \mathcal{E}$
Υ	Set of dispatchable units, $\Upsilon = \{1, \dots, \upsilon, \dots, \Upsilon\}$
Ψ	Set of non-dispatchable units, $\Psi = \{1, \dots, \psi, \dots, \Psi\}$
ϕ	Set of storage units, $\phi = \{1, \dots, \Phi, \dots, \phi\}$
Ω	Set of scenarios, $\Omega = \{1, \dots, \omega, \dots, \Omega\}$
K	Set of segments, $\mathrm{K} = \{1, \dots, k, \dots, K\}$
State Variables	
M	Big number
η	Storage unit's efficiency
$\rho^{\min}$	Minimum MG power factor
C^{util}, C^{int}	Utility and interruption cost
$\alpha^{int}, \beta^{int}$	Percent interruption at node and day
$c_1^{\upsilon}, c_2^{\upsilon}, c_3^{\upsilon}$	Operational cost parameters for dispatchable unit υ
$D_{\zeta i}$	Apparent demand from appliance ζ at node i
$Y_{\upsilon t}^{k}$	Maximum power from dispatchable unit υ in segment k at time t
$c_{\upsilon}^{up}, c_{\upsilon}^{down}$	Start-up and shut-down cost parameters for dispatchable unit υ
$c_{\upsilon}^{intercept}$	Intercept cost parameters for dispatchable unit υ
$c_{\upsilon k}^{slope}$	slope cost parameter for dispatchable unit υ in segment k
$I_{\upsilon}^{emiss.}$	Intercept emission parameter for dispatchable unit υ
$S^{emiss.}{}_{\upsilon}^{k}$	slope emission parameter for dispatchable unit υ in segment k
$UT_{\upsilon}^{min}, DT_{\upsilon}^{min}$	Minimum up and down time for dispatchable unit υ
$P_{\upsilon}^{min}, P_{\upsilon}^{max}$	Minimum and maximum active power from dispatchable unit υ
$Q_{\upsilon}^{min}, Q_{\upsilon}^{max}$	Minimum and maximum reactive power from dispatchable unit υ
$R_{\upsilon}^{up}, R_{\upsilon}^{down}$	Ramp-up and ramp-down rates for dispatchable unit υ
R_{ij}, X_{ij}	Resistance and reactance of line i, j where $(i, j) \in \mathcal{E}$
$I_{ij}^{\max}$	Maximum current for line i, j where $(i, j) \in \mathcal{E}$
$SOC_{\Phi}^{min}, SOC_{\Phi}^{max}$	Minimum and maximum state of charge levels for storage unit Φ
V_i^{min}, V_i^{max}	Minimum and maximum squared voltage levels for node i
C_i^{min}, C_i^{max}	Minimum and maximum capacitor size at node i
$\mathrm{E}_t^{min}, \mathrm{E}_t^{max}$	Minimum and maximum power exchange at time t
H_t	Microgrid inertia at time t
h_{υ}, h_{Φ}	Inertial constant for dispatchable unit υ and storage unit Φ
$\Delta f^{max}, \Delta f^{min}$	Minimum and maximum rate of change of frequency
F	Nominal frequency set point
F^{max}, F^{min}	Minimum and maximum nominal frequency

Table 2b: Nomenclature for proposed MG dispatch policy

Exogenous Variables	
$p_{it}^{\omega}, q_{it}^{\omega}$	Active and reactive power demand at bus i at time t in scenario ω
$n_{\psi t}^{\omega}$	Active power generation from non-dispatchable unit ψ at time t in scenario ω
Binary Decision Variables	
$c_{\Phi t}^{\omega}$	Charging/discharging status of storage unit Φ at time t in scenario ω
$u_{\upsilon t}^{\omega}$, $d_{\upsilon t}^{\omega}$	Start-up/shut down indicator for dispatchable unit υ at time t in scenario ω
$s_{\upsilon t}^{\omega}$	Status (on/off) indicator of dispatchable unit υ at time t in scenario ω
$A_{\zeta i}^{\omega}$	Status (on/off) indicator of appliance ζ at node i in scenario ω
Continuous Decision Variables	
$G_{\upsilon t}^{k\omega}$	Apparent power generation from dispatchable unit υ in segment k at time t in scenario ω
$P_{\upsilon t}^{\omega}, Q_{\upsilon t}^{\omega}$	Active and reactive power generation from dispatchable unit υ at time t in scenario ω
$b_{\Phi t}^{\omega}$	Active power generation from storage unit Φ at time t in scenario ω
$B_{\Phi t}^{\omega}$	Apparent power generation from storage unit Φ at time t in scenario ω
$o_{\Phi t}^{\omega}, d_{\Phi t}^{\omega}$	Auxiliary charge and discharge variables for $B_{\Phi t}^{\omega}$ in scenario ω
V_{it}^{ω}	Squared voltage and capacitive reactance at node i at time t in scenario ω
I_{ij}^{ω}	Current through line i,j at time t where $(i,j) \in \mathcal{E}$ in scenario ω
$P_{i,j}^{\omega t}, Q_{i,j}^{\omega t}$	Active and reactive power flow through line i,j at time t, where $(i,j) \in \mathcal{E}$ in scenario ω
χ_{it}^{ω}	Capacitive reactance at node i at time t in scenario ω
Γ_{it}^{ω}	Interrupted demand at node i at time t in scenario ω
U_{t}^{ω}	Apparent power from external utility grid at time t in scenario ω
$L_{t}^{\omega}, W_{t}^{\omega}$	Active and reactive power generation from the external utility at time t in scenario ω
Δf_t	Amount of frequency deviation during islanding at time t
δ_t	Rate of change of frequency during islanding at time t

The nomenclature in **Table 2** is used to formulate the proposed MG dispatch policy as a MILP to capture the AC-UC problem. The challenges of MG dispatch outlined in **Table 1** are considered in the proposed MG dispatch policy, including linearized AC power flow physics equations, UC under supply and demand uncertainty, PF correction using DSM, and frequency control.

2.2 Proposed MG Dispatch Policy for AC-UC Problem

In this section, we formulate our proposed MG dispatch model using the nomenclature in **Table 2**. The purpose of the MG dispatch policy is to describe the behavior of an MG system (see **Figure 1**), where we seek to model the effect of poor power quality on an MG's operating efficiency and stability while simultaneously considering the logistics of power transfer.

Within the proposed MG dispatch policy, there are two conflicting objectives. The first objective is to minimize the total operational cost consisting of fuel, start-up, shut-down, external utility, and interruption costs. The second objective is to minimize the amount of CO_2 emissions produced during energy production. The costs and emissions produced from dispatchable units are modeled with a quadratic function (3). Therefore, (3) is linearized using piecewise linear approximation (PLA) [17], where the resulting objective functions and constraint sets describing the piecewise functions are shown in (4) to (7). An advantage of PLA is the computational efficiency gained when obtaining solutions for a segment instead of every point along a function. Moreover, PLA uses a dynamic mechanism for segmentation to estimate various function behaviors accurately. It should be noted that this is a minimization problem since $c_1^{\upsilon} > 0$, and no binary variables are necessary to link the segments in the piecewise linear function. Notably, the linearized cost and emission functions are a conservative overestimation to consider the worst possible scenario for a convex minimization function.

$$\text{Min } z = \mathbf{E}\left[\sum_{\omega\in\Omega} P(\omega) \times \sum_{\upsilon\in\Upsilon}(c_1^{\upsilon}(P_{\upsilon t}^{\omega})^2 + c_2^{\upsilon}P_{\upsilon t}^{\omega} + c_3^{\upsilon})\right] \tag{3}$$

$$\min \mathbf{E}\left[\sum_{\omega\in\Omega} P(\omega) \times \left(\begin{array}{c}\sum_{\upsilon\in\Upsilon}\left(c_{\upsilon}^{intercept} s_{\upsilon t}^{\omega} + \sum_{k=1}^{\mathrm{K}} P_{\upsilon t}^{\omega}\, c_{\upsilon k}^{slope}\right) + \\ \sum_{t\in\mathcal{T}}\sum_{i\in\mathcal{N}}\sum_{\zeta\in Z} c_{\upsilon}^{up} u_{\upsilon t}^{\omega} + c_{\upsilon}^{down} d_{\upsilon t}^{\omega} + C^{util} U_t^{\omega} + C^{int} D_{\zeta i}\end{array}\right)\right] \tag{4}$$

$$\min \mathbf{E}\left[\sum_{\omega\in\Omega} P(\omega) \times \sum_{\upsilon\in\Upsilon}\left(I_{\upsilon}^{emiss.} s_{\upsilon t}^{\omega} + \sum_{k=1}^{\mathrm{K}} P_{\upsilon t}^{\omega}\, S^{emiss.\,k}_{\upsilon}\right)\right] \tag{5}$$

$$\sum_{k=1}^{\mathrm{K}} G_{\upsilon t}^{\mathrm{k}\omega} = P_{\upsilon t}^{\omega} \qquad \forall\, \upsilon \in \Upsilon, t \in \mathcal{T}, \mathrm{k} \in K, \omega \in \Omega \tag{6}$$

$$G_{\upsilon t}^{\mathrm{k}\omega} \le Y_{\upsilon t}^{k} \qquad \forall\, \upsilon \in \Upsilon, t \in \mathcal{T},\ \mathrm{k} \in \{1,\ \ldots,\ K-1\}, \omega \in \Omega \tag{7}$$

The MG system (see **Figure 1**) shows a point of coupling between supply on the left and demand on the right. Constraint sets (8) and (9) model the nodal power balance between bus i and j of the admittance matrix. In other words, these constraints describe the power balance between supply (e.g., solar panels, wind turbine) and demand nodes (e.g., residential, commercial) within the MG system. The forecasted generation from non-dispatchable units (i.e., solar panels and wind turbines) is treated as a parameter in the MILP. The constraint set (10) represents the linearized AC power flow physics [44]. The branch current (L_{ij}) is not considered in the updated *LinDistFlow* equations by [45]. In *LinDistFlow* equations, the impact of current is defined as the sum of squares of resistance and reactance $\left(\mathrm{R}_{ij}^2 + \mathrm{X}_{ij}^2\right)$. Since this term is negligible in (10), it is removed from the updated *LinDistFlow* equations. While (11) ensures that the line voltage limits are met during operation, (12) ensures that the capacitive reactance remains within its upper and lower limits. The relationship between voltage, current, active, and reactive power flows is modeled in (13). We use the upper and lower voltage limits for computational tractability to relax the non-convex equality constraint (13) into the inequality constraint (14). Next, (14) is linearized using inner and outer approximation methods by [46] to develop a second-order cone model for the stochastic AC-UC problem. Finally, (15) ensures that current limits are met throughout the transmission lines.

$$\sum_{\psi\in\Psi\{i\}} n_{\psi t}^{\omega} + \sum_{\Phi\in\phi\{i\}} o_{\Phi t}^{\omega} - d_{\Phi t}^{\omega} + \sum_{\upsilon\in\Upsilon\{i\}} P_{\upsilon t}^{\omega} - (p_{it}^{\omega} - \Gamma_{it}^{\omega}) + L_t^{\omega} = \sum_{\substack{(i,j)\in\mathcal{E} \\ j\in\mathcal{N}(i)}} P_{i,j}^{\omega \mathrm{t}} \qquad \begin{array}{c}\forall\, i \in \mathcal{N}, \\ t \in \mathcal{T}, \omega \in \Omega\end{array} \tag{8}$$

$$\sum_{\upsilon\in\Upsilon\{i\}} Q_{\upsilon t}^{\omega} - (q_{it}^{\omega} - \chi_{it}^{\omega}) + W_t^{\omega} = \sum_{\substack{(i,j)\in\mathcal{E} \\ j\in\mathcal{N}\{i\}}} Q_{i,j}^{\omega \mathrm{t}} \qquad \begin{array}{c}\forall\, i \in \mathcal{N}, \\ t \in \mathcal{T}, \omega \in \Omega\end{array} \tag{9}$$

$$V_{jt}^{\omega} = V_{it}^{\omega} - 2\left(\mathrm{R}_{ij} P_{i,j}^{\omega \mathrm{t}} + \mathrm{X}_{ij} Q_{i,j}^{\omega \mathrm{t}}\right) + \left(\mathrm{R}_{ij}^2 + \mathrm{X}_{ij}^2\right) I_{ij}^{\omega} \qquad \forall\, (i,j) \in \mathcal{E}, t \in \mathcal{T}, \omega \in \Omega \tag{10}$$

$$V_i^{min} \le V_{it}^{\omega} \le V_i^{max} \qquad \forall\, i \in \mathcal{N}, t \in \mathcal{T}, \omega \in \Omega \tag{11}$$

$$C_i^{min} \le \chi_{it}^{\omega} \le C_i^{max} \qquad \forall\, i \in \mathcal{N}, t \in \mathcal{T}, \omega \in \Omega \qquad (12)$$

$$I_{ij}^{\omega} = \frac{(P_{i,j}^{\omega t})^2 + (Q_{i,j}^{\omega t})^2}{V_{it}^{\omega}} \qquad \forall\, (i,j) \in \mathcal{E}, t \in \mathcal{T}, \omega \in \Omega \qquad (13)$$

$$V_i^{min} \le (P_{i,j}^{\omega t})^2 + (Q_{i,j}^{\omega t})^2 \le V_i^{max} \qquad \forall\, (i,j) \in \mathcal{E}, t \in \mathcal{T}, \omega \in \Omega \qquad (14)$$

$$I_{ij}^{\omega} \le I_{ij}^{\max} \qquad \forall\, (i,j) \in \mathcal{E}, t \in \mathcal{T}, \omega \in \Omega \qquad (15)$$

The MG system (see **Figure 1**) shows transmission infrastructure that transfers apparent power from supply to demand nodes. Power quality describes the efficiency of the MG system to ensure that the real/true/active component of apparent power produced far exceeds the reactive component. DSM is used to regulate the power quality throughout the transmission lines, preventing power loss due to heat dissipation during transmission instead of being consumed by the demand nodes. Constraint (16) defines auxiliary variables for active and reactive power from an external utility, while (17) enforces upper and lower limits on power purchased from the external utility. Constraint sets (18) to (19) model a flexible load-shedding program where the hourly percentage regulates the maximum load shed at each bus (α^{int}) and daily percentage (β^{int}). Constraint (20) ensures that enough static appliances are turned off to satisfy the load shedding required to sustain the desired PF and MG stability. The PF is confined to its upper and lower limits in (21), while (22) describes the PF in terms of a non-linear relationship between active and reactive power. Constraint (22) is the linearized form of a second-order cone model to constraint set (23) to (24) by assigning a PF value to the entire MG system. The contribution from capacitive reactance is included in (23) since this class of DERs has units at each bus. Finally, (23) to (24) ensure the desired power quality is sustained throughout the transmission lines, and DERs with the assigned PF are used to produce energy.

$$U_t^{\omega} = L_t^{\omega} + W_t^{\omega} \qquad t \in \mathcal{T}, \omega \in \Omega \qquad (16)$$

$$\mathrm{E}_t^{min} \le U_t^{\omega} \le \mathrm{E}_t^{max} \qquad t \in \mathcal{T}, \omega \in \Omega \qquad (17)$$

$$\sum_{t \in \mathcal{T}} \Gamma_{it}^{\omega} \le \beta^{int} \sum_{t \in \mathcal{T}} p_{it}^{\omega} \qquad \forall\, i \in \mathcal{N}, \omega \in \Omega \qquad (18)$$

$$\Gamma_{it}^{\omega} \le \alpha^{int} p_{it}^{\omega} \qquad \forall\, i \in \mathcal{N}, t \in \mathcal{T}, \omega \in \Omega \qquad (19)$$

$$\sum_{\zeta \in Z} D_{\zeta i} A_{\zeta i}^{\omega} \ge \Gamma_i^{\omega} \qquad \forall\, i \in \mathcal{N}, \omega \in \Omega \qquad (20)$$

$$pf^{min} \le cos\phi \le 1 \qquad \forall\, (i,j) \in \mathcal{E}, t \in \mathcal{T}, \omega \in \Omega \qquad (21)$$

$$cos\phi = \frac{P_{i,j}^{\omega t}}{\sqrt{(P_{i,j}^{\omega t})^2 + (Q_{i,j}^{\omega t})^2}} \qquad \forall\, (i,j) \in \mathcal{E}, t \in \mathcal{T}, \omega \in \Omega \qquad (22)$$

$$pf^{min}(Q_{i,j}^{\omega t} + \chi_{it}^{\omega}) \le \sqrt{1 - pf^{min^2}} \cdot P_{i,j}^{\omega t} \qquad \forall\, (i,j) \in \mathcal{E}, t \in \mathcal{T}, \omega \in \Omega \qquad (23)$$

$$pf^{min} \cdot Q_{\upsilon t}^{\omega} \le \sqrt{1 - pf^{min^2}} \cdot P_{\upsilon t}^{\omega} \qquad \forall\, \upsilon \in \Upsilon\ , t \in \mathcal{T}, \omega \in \Omega \qquad (24)$$

Dispatchable units are controllable supply nodes the main utility can readily deploy to meet current demand. These dispatchable units are often diesel or synchronous generators (see **Figure 1**) since fossil fuels can be readily converted to energy despite their environmental impact. Constraints (25) and (26) represent the active and reactive power generation limits. These constraints also ensure that only committed units can generate power ($s_{\upsilon t}^{\omega} = 1$). The relationship between subsequent planning horizons while considering the minimum up and down time for dispatchable units is modeled in constraints (27) to (29). The relationship between start-up, shut-down, and status indicator for each dispatchable unit throughout the planning horizon is formulated in constraints (30) and (31). Finally, the ramp-up and ramp-down limits are enforced in constraints (32) and (33).

$$P_{\upsilon}^{min} \leq P_{\upsilon t}^{\omega} \leq P_{\upsilon}^{max} s_{\upsilon t}^{\omega} \qquad \forall\, \upsilon \in \Upsilon, t \in \mathcal{T}, \omega \in \Omega \qquad (25)$$

$$Q_{\upsilon}^{min} \leq, Q_{\upsilon t}^{\omega} \leq Q_{\upsilon}^{max} s_{\upsilon t}^{\omega} \qquad \forall\, \upsilon \in \Upsilon, t \in \mathcal{T}, \omega \in \Omega \qquad (26)$$

$$\sum_{k=24-(UT_{\upsilon}^{min}-t)}^{24} \mathcal{u}_{\upsilon k}^{\omega} \leq M s_{\upsilon t}^{\omega} \qquad \forall\, \upsilon \in \Upsilon, t \in \{1, \dots, UT_{\upsilon}^{min}\}, \omega \in \Omega \qquad (27)$$

$$\sum_{k=24-(DT_{\upsilon}^{min}-t)}^{24} d_{\upsilon k}^{\omega} \leq M(1 - s_{\upsilon t}^{\omega}) \qquad \forall\, \upsilon \in \Upsilon, t \in \{1, \dots, DT_{\upsilon}^{min}\}, \omega \in \Omega \qquad (28)$$

$$s_{\upsilon 1}^{\omega} = s_{\upsilon 24}^{\omega} + \mathcal{u}_{\upsilon 1}^{\omega} - d_{\upsilon 1}^{\omega} \qquad \forall\, \upsilon \in \Upsilon, \omega \in \Omega \qquad (29)$$

$$s_{\upsilon t}^{\omega} = s_{\upsilon t-1}^{\omega} + \mathcal{u}_{\upsilon t}^{\omega} - d_{\upsilon t}^{\omega} \qquad \forall\, \upsilon \in \Upsilon, t \in \mathcal{T}, \omega \in \Omega \qquad (30)$$

$$\mathcal{u}_{\upsilon t}^{\omega} + d_{\upsilon t}^{\omega} \leq 1 \qquad \forall\, \upsilon \in \Upsilon, t \in \mathcal{T}, \omega \in \Omega \qquad (31)$$

$$R_{\upsilon}^{down} \geq G_{\upsilon t-1}^{\omega} - G_{\upsilon t}^{\omega} \qquad \forall\, \upsilon \in \Upsilon, t \in \mathcal{T}, \omega \in \Omega \qquad (32)$$

$$R_{\upsilon}^{up} \geq G_{\upsilon t}^{\omega} - G_{\upsilon t-1}^{\omega} \qquad \forall\, \upsilon \in \Upsilon, t \in \mathcal{T}, \omega \in \Omega \qquad (33)$$

Storage units are dispatchable, but this resource's state alternates between supply and demand based on whether the unit is discharging or charging (see **Figure 1**). Like non-dispatchable units, storage units are assumed to operate at unity PF and can only provide active power. A storage unit's SOC is represented in (34). Here, the round-trip efficiency (η) is calculated based on the status of the battery (charging or discharging). Auxiliary variables ($d_{\Phi t}^{\omega}, o_{\Phi t}^{\omega}$) denote the SOC for discharging and charging power in (35). Constraint sets (36) to (38) link the auxiliary variables to the status of the storage unit. Here, the binary variable ($c_{\Phi t}^{\omega}$) ensures the storage unit cannot be charging and discharging simultaneously. Constraint (38) is the linearized version of (34). The SOC limit is enforced in (39). In the proposed MG dispatch policy, we assume that battery SOC is full at the beginning of the planning horizon ($t = 0$) and it is full at end of the scheduling horizon ($t = \mathcal{T}$).

$$b_{\Phi t+1}^{\omega} = \begin{cases} b_{\Phi t}^{\omega} - \eta B_{\Phi t}^{\omega}, & \text{if charging} \\ b_{\Phi t}^{\omega} - \frac{1}{\eta} B_{\Phi t}^{\omega}, & \text{if discharging} \end{cases} \qquad \forall\, \Phi \in \phi, t \in \mathcal{T}, \omega \in \Omega \qquad (34)$$

$$B_{\Phi t}^{\omega} = d_{\Phi t}^{\omega} - o_{\Phi t}^{\omega} \qquad \forall\, \Phi \in \phi, t \in \mathcal{T}, \omega \in \Omega \qquad (35)$$

$$M(1 - c_{\Phi t}^{\omega}) \geq d_{\Phi t}^{\omega} \qquad \forall\, \Phi \in \phi, t \in \mathcal{T}, \omega \in \Omega \qquad (36)$$

$$M c_{\Phi t}^{\omega} \geq o_{\Phi t}^{\omega} \qquad \forall\, \Phi \in \phi, t \in \mathcal{T}, \omega \in \Omega \qquad (37)$$

$$b_{\Phi t+1}^{\omega} = b_{\Phi t}^{\omega} - \frac{d_{\Phi t}^{\omega}}{\eta} + \eta o_{\Phi t}^{\omega} \qquad \forall\, \Phi \in \phi, t \in \mathcal{T}, \omega \in \Omega \qquad (38)$$

$$SOC_{\Phi}^{min} \leq b_{\Phi t}^{\omega} \leq SOC_{\Phi}^{max} \qquad \forall\, \Phi \in \phi, t \in \mathcal{T}, \omega \in \Omega \qquad (39)$$

In addition to the logistical constraints of power transfer, another set of constraints used to capture the MG's stability are as follows: Both the MG inertia and RF are defined in (40) and (41), respectively. These metrics are derived from the swing equation, which governs the rotary dynamics of synchronous generators [26]. Constraint (42) ensures that the post-fault RF remains within its upper and lower limits. The MG frequency deviation is calculated in (43), where τ is the step within time t for sampling the deviations. Similarly, (44) ensures MG frequency deviations remain within acceptable limits to ensure grid stability and avoid tripping protection relays.

$$H_t = \frac{\left[\sum_{\upsilon \in \Upsilon} P_{\upsilon}^{max} h_{\upsilon} + \sum_{\Phi \in \phi} SOC_{\Phi}^{max} h_{\Phi}\right]}{F} \qquad \forall\, t \in \mathcal{T} \qquad (40)$$

$$\delta_t = \frac{\left[\begin{matrix} \sum_{\upsilon \in \Upsilon} \Delta P_{\upsilon t}^{\omega} \\ + \sum_{\Phi \in \phi} \Delta b_{\Phi t}^{\omega} - \Delta f_{t-1} - U_t^{\omega} \end{matrix}\right]}{2H_t} \qquad \forall\, t \in \mathcal{T}, \omega \in \Omega \qquad (41)$$

$$\Delta f^{min} \leq \delta_t \leq \Delta f^{max} \qquad \forall\, t \in \mathcal{T} \qquad (42)$$

$$\Delta f_t = \Delta f_{t-1} + \delta_t \tau \qquad \forall\, t \in \mathcal{T} \qquad (43)$$

$$F^{min} \leq \Delta f_t \leq F^{max} \qquad \forall\, t \in \mathcal{T} \qquad (44)$$

The above AC-UC problem is formulated as a MILP to optimize the MG's operational efficiency by scheduling various DERs according to the incentive-based DSM program. This allows the TSO to minimize the total operational cost while considering power flow physics, the mechanical limitation of each type of DER, and the influence of both internal market forces and external climate forces. A rolling horizon heuristic decomposes the original AC-UC problem into smaller sub-problems, which are solved sequentially throughout the entire scheduling horizon. Notably, there is overlap along the sequence of sub-problems to preserve information.

2.3 Proposed Rolling Horizon Heuristic with ϵ - Constraint Method

The rolling horizon approach is a reactive scheduling formulation that iteratively solves the AC-UC problem defined in (3) to (44) by incrementing over the entire time horizon [33]. Thus, it is assumed that the input data from the MG system is constantly being fed to the MILP, and all parameters become known at time (t). Since the computational complexity of this problem is directly proportional to the length of the time horizon, the rolling horizon approach segments the overall time horizon into more tractable sub-horizons, as illustrated in **Figure 2**.

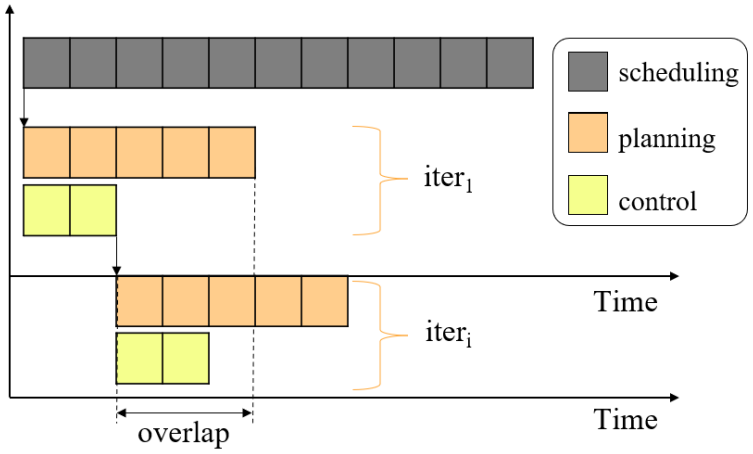

Figure 2: Reactive scheduling via a rolling horizon approach

In **Figure 2**, the scheduling horizon (SH) denotes the overall time horizon. At the same time, perfect information is assumed during the planning horizon (PH), and the final dispatch decisions are retained along the control horizon (CH). Since solving the AC-UC problem over the entire SH is infeasible, the SH is decomposed into subsections called PHs, where a feasible solution can be obtained. However, there is a risk that solutions obtained along the PHs may not be feasible along the overall SH. Thus, a certain amount of overlap is required between PHs to ensure the solutions obtained in each iteration remain applicable to the original AC-UC problem defined over the SH. Here, theorem three by [47] is used to determine an appropriate amount of overlap required between PHs. During the first iteration of the rolling horizon heuristic, the initial MG system's state is used to obtain DER schedules along the first PH. The MG system's state at the end of the resulting CH within the overlap is fixed and used to iteratively plan for subsequent PHs until the end of the SH. This reactive scheduling formulation allows for near real-time dispatch within the MG system for short-term tactical planning. The rolling horizon approach is summarized in **Table** 3 and visually illustrated in **Figure 3**.

Table 3: Rolling horizon heuristic for MG dispatch

Input: SH, PH, CH
1: SH for day-ahead scheduling
2: calculate the number of sub-problems i such that $tot_i = (SH - PH + CH)/CH$
3: calculate the overlap of sub-problems o such that $tot_o = 2 * CH - 1$
4: update the MILP parameters to reflect the current MG state
5: solve MG dispatch policy for current PH using the ϵ-constraint method
6: store dispatch decisions for the current CH
7: **if** $i == tot_i$:
8: **terminate**

9: **else if** current PH infeasible:
10: **while** current PH is infeasible:
11: adjust the DSM program by relaxing constraints (18) – (20)
12: **repeat** steps 4 to 6
13: **else**:
14: $i \mathrel{+}= 1$
15: **repeat** steps 4 to 6
Output: exact solutions for each CH along the overall SH

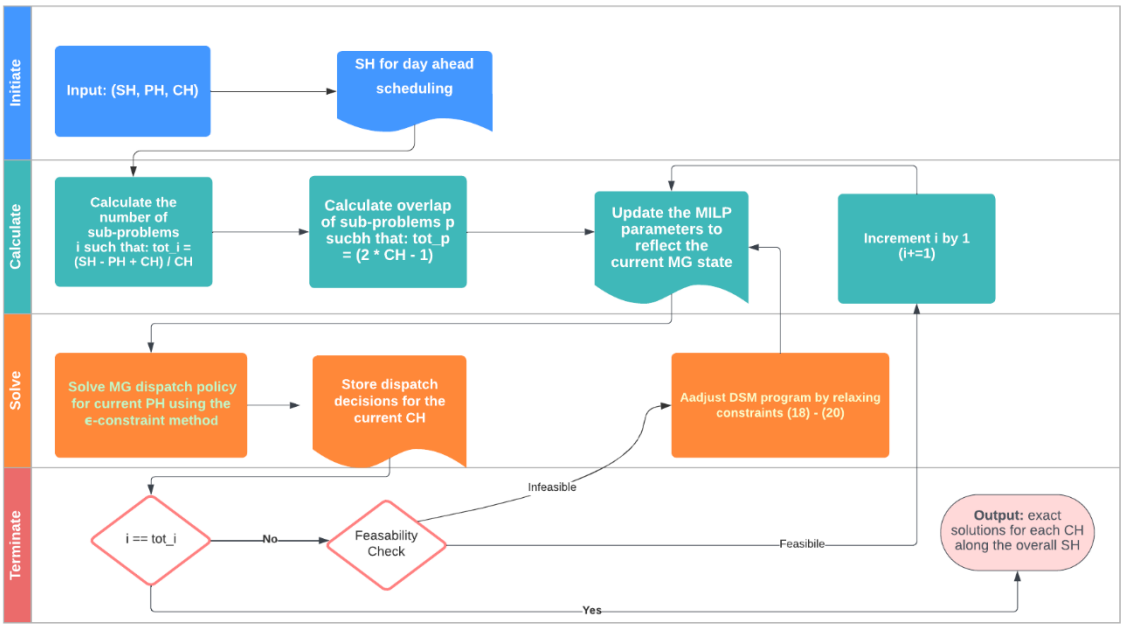

Figure 3: Rolling horizon heuristic for MG dispatch

Initially, we defined the scheduling, planning, and control horizons as input into the rolling horizon heuristic algorithm. Next, in Steps 1-2, we calculated the number of sub-problems or iterations, and then we calculated the overlap in Step 3 to ensure information is shared across PHs between iterations. Subsequently, we updated the MILP parameters in Step 4 and solved the MG dispatch policy for the current PH in Step 5. Next, the dispatch decisions for the current CH are fixed and used to define the start of successive PHs in Step 6. If the current sub-problem corresponds to the final iteration, the process ends in Steps 7 to 8. However, if the current sub-problem is infeasible, tunable DSM parameters in (18) to (20) are adjusted until a feasible solution is obtained in Steps 9 to 12. Otherwise, the dispatch decisions obtained during the current iteration are fixed along the CH, and this process repeats until solutions are obtained for the original SH in Steps 13 to 15.

Since solutions are fixed along the CH, the conflicting objectives (4) and (5) must be resolved along the CH and derive a set of trade-off solutions for a given scenario. The Pareto frontier for each sub-problem is generated in Step 5 by the ε-constraint method and is used to select non-dominated solutions [48]. The ϵ-constraint method to solve the proposed MG dispatch policy was first introduced by [20]. The ϵ-constraint method generates a Pareto frontier for a multi-objective problem by solving a sequence of single-objective problems. Here, the secondary objective (5) is embedded as a constraint in a single objective problem. In

the ϵ-constraint method, the first step is finding each objective function's lower and upper bounds. These values were obtained by first solving the multi-objective as a single-objective optimization problem, prioritizing each objective function separately.

$$\mathbf{E}\left[\sum_{\omega\in\Omega} P(\omega)\times\sum_{\upsilon\in\Upsilon}\left(I_{\upsilon}^{emiss.}s_{\upsilon t}^{\omega}+\sum_{k=1}^{\mathrm{K}}P_{\upsilon t}^{\omega}\,S^{emiss.}{}_{\upsilon}^{k}\right)\right]\geq RHS_{emission} \qquad (45)$$

After adding (5) as constraint (45), the proposed MG dispatch policy is then solved for the primary objective (4) while tightening (45). Here, (45) is divided into equal intervals where the primary objective (4) is solved for (n) different right-hand side values to generate the Pareto Front. The ε-constraint algorithm is summarized in **Table 4** and visually illustrated in **Figure 4**.

Table 4: ε-constraint method for multi-objective optimization

Input: n intervals, i iterations, $RHS_{emission}$
1: $\varepsilon = -RHS_{emission}/n$
2: **while** $RHS_{emission} > 0$:
3: solve MG dispatch policy
4: $RHS_{emission} = RHS_{emission} + \varepsilon$
5: print i : cost, emissions
Output: Pareto font of cost and emission trade-off solutions

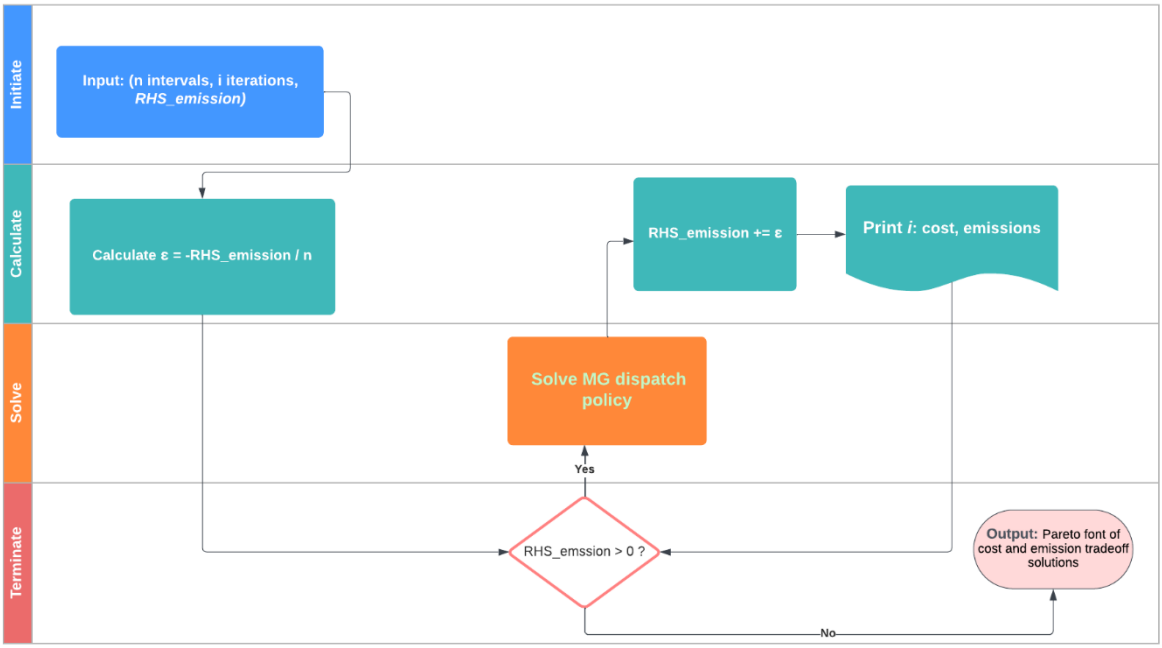

Figure 4: ε-constraint method for multi-objective optimization

Each compromised solution along the Pareto Front between the conflicting objectives of cost and emission is subject to the uncertainty of both internal market forces and external climate forces. Thus, the multi-

objective complexity of the AC-UC problem defined in (3) to (44) is compounded under these stochastic conditions.

3 RESULTS

Our proposed MG dispatch policy was tested for efficiency, scalability, and resiliency. The IEEE 18-bus and IEEE 30-bus characteristics were both obtained from [13], [43], [49]. The IEEE 30-bus test case represents a simple approximation of the American Electric Power system [50] in December 1961. Both MGs have a radial topology where the dispatchable and storage units are located at the reference (slack bus) while the non-dispatchable units are distributed throughout the network. Storage units have a round-trip efficiency of 0.95 in both MGs. The amount of demand and capacitance for all consumers participating in the utility's DSM program is controllable at each bus. Our proposed MG dispatch policy was coded in AMPL software and solved using CPLEX 12.1 solver on a desktop computer with Intel i7 2.67 GHz and 16 GB of RAM for replicability purposes.

3.1 Solution Scalability for MGs via a Rolling Horizon Approach

The proposed MG dispatch policy is formulated with a day-ahead SH. Thus, we assumed uncertain parameters were updated at 15-minute intervals along the hourly CH for near real-time dispatch. We included information from the previous PH in the following PH via available DERs while ensuring the overall AC-UC problem remains feasible along the SH. In order to assess the computational efficiency across different problem instances, the contribution of busses within both MGs was included incrementally, starting from the slack bus to nodes at the edge of each MG. The computational efficiency will also depend on the chosen PH and the number of sub-problems. Since a PH the length of 24-time intervals equates to solving the AC-UC problem over the SH, it is considered the base case as described in **Table 5.**

Table 5: Solution times for the IEEE 18-bus and IEEE 30-bus networks with varying PHs.

PH	3	6	9	12	15	18	21	24
tot_i	12	10	9	7	6	4	3	1
MG Size	CPU Times (s)							
6-bus	0.52	0.48	0.45	0.44	0.35	0.28	0.19	**1.0**
9-bus	0.74	0.76	0.69	0.55	0.42	**1.0**	0.23	0.12
18-bus	0.89	0.84	0.75	0.65	0.53	**1.0**	0.36	0.21
24-bus	1.13	1.03	1.08	1.03	**1.0**	0.78	0.67	0.51
27-bus	1.53	1.57	1.48	1.11	1.02	**1.0**	0.77	0.63
30-bus	1.91	1.75	1.55	**1.0**	1.11	1.08	1.05	1.03

Table 5 shows the average CPU time to obtain an optimal solution for varying problem instances. Here, a value of 1.0 denotes the best average solve time for a given problem instance. Since solve time is proportional to the problem instance, larger problems intuitively take longer than smaller ones. The solve time is also proportional to the number of sub-problems for a given PH. For example, the 27-bus instance can be solved in 0.63s in the base case when considering the entire SH but takes 1.53s if this problem instance is split into 12 smaller sub-problems. However, the benefit of decomposing the problem into smaller pieces is seen at four sub-problems since the best solve time is obtained. The randomness of varying solve time is based on the solver's starting point or proximity to the optimal solution (optimality gap) within the proposed heuristic. The starting point is fixed for a given problem instance based on the optimality gap to ensure consistent solutions and robustness. Thus, computational efficiency can be improved by

constantly tuning the rolling horizon heuristic. This study uses the rolling horizon approach with the ε-constraint method to obtain non-dominated solutions iteratively with computational efficiency.

After determining the appropriate number of sub-problems (or PHs) based on the problem instance (or MG size), the primary objective (4) was divided into 50 equidistant intervals. The proposed MG dispatch policy was solved sequentially at each interval by tightening (45) to produce the corresponding Pareto Front. The Pareto Frontier for both the IEEE 18-bus and IEEE 30-bus are illustrated in **Figure 5**.

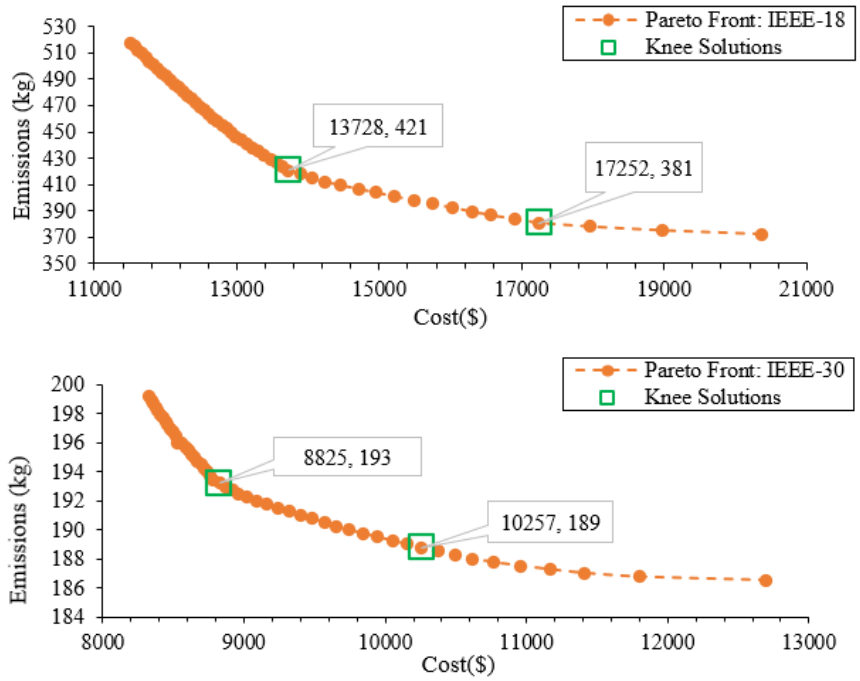

Figure 5: Pareto Frontier of MG dispatch policy for IEEE 18-bus (top) and IEEE 33-bus (bottom)

The cost function was selected as the primary objective in the ϵ-constraint method and ranged from [11515, 20365] for the IEEE 18-bus and [8329, 12697] for the IEEE 30-bus. Likewise, when selected as the primary objective, the emissions function ranged from [372, 518] for the IEEE18-bus and [187, 199] for the IEEE 30-bus. The preferred trade-off solution in the Pareto Frontier is selected by determining the knee solutions using [48]. Knee solutions are points with a larger derivative than others, indicating a change in the Pareto Front's trajectory and, consequently, a non-dominated solution between the vector components. The best compromise or knee solution was chosen in terms of cost for the IEEE 18-bus and IEEE 30-bus, respectively. The first knee solution in the IEEE 18-bus illustrates a 66% reduction in CO_2 emissions for a 19% increase in cost. Similarly, the IEEE 30-bus illustrates a 50% reduction in CO_2 emissions for a 12% increase in operational cost. Both MGs show a significant reduction of CO_2 emissions under the proposed MG dispatch policy for a marginal increase in the total operational cost.

3.2 MG Efficiency via Load Reduction & Power Quality

Since the utility would have to supply more energy to an MG system with a poor PF, industrial consumers are encouraged to use more energy-efficient equipment or absorb the cost of their equipment's inefficiency. A sensitivity analysis with a PF range of [0.95, 0.9, 0.85, and 0.8] is conducted to investigate an MG's efficiency using the proposed MG dispatch policy.

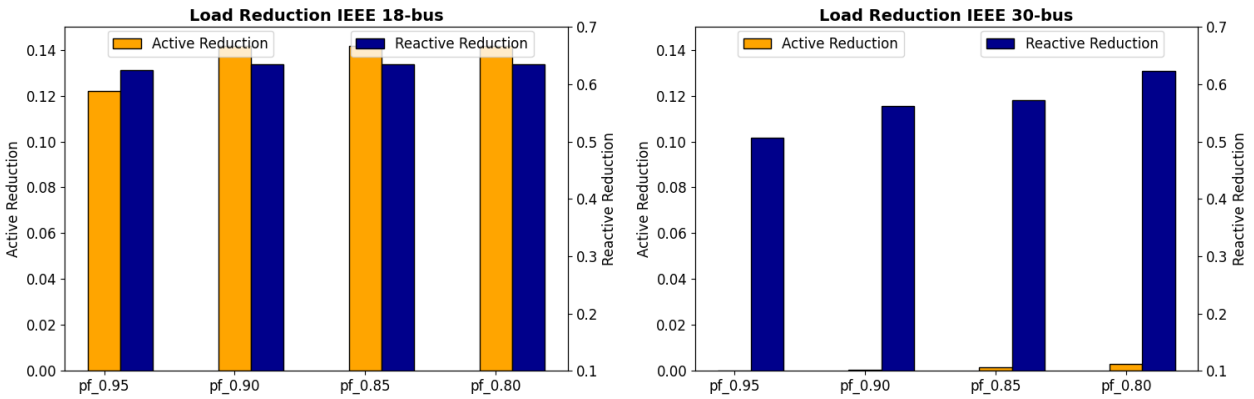

Figure 6: Portion of active and reactive demand reduction at various power factor across both the IEEE 18-bus (left) and IEEE 30-bus (right)

Figure 6 illustrates the reduced active and reactive demand portions under the proposed MG dispatch policy. Here, reactive demand is reduced by roughly 60% for all PFs in the IEEE 18-bus compared to the 30% load reduction observed in [36]. The portion of demand reduction in the IEEE 18-bus initially appears to be independent of PF except at a PF of 0.95, with a smaller reduction of active demand. Thus, we see a slight improvement in the MG network's efficiency compared to the other PF values. Since unity (PF = 1) is achieved at a 100% reduction of the reactive demand, the improvement in power quality becomes more apparent across PFs in the IEEE 30-bus network. At a PF of 0.95 in IEEE 30-bus, there is no reduction to the active demand (load shedding) from consumers; only the reactive demand is reduced. Thus, the IEEE 30-bus has a lower operating cost than the IEEE 18-bus and requires significantly less load shedding under the utility's DSM program. Since the standard electrical code according to [51] requires a PF between [0.8, 1] for MG operation, we conservatively set PF to 0.95 for further analysis throughout this study to observe each MG's behavior while operating efficiently.

Despite an MG operating at a high efficiency, traditional market forces such as supply and demand are critical factors in the economics and sustainability of MG operations. Stochastic active and reactive power generated from the dispatchable units is assumed to be stored before being released into the MG. A sensitivity analysis is used to investigate the scalability and resiliency of our proposed MG dispatch policy by applying demand and supply shocks to both MGs outlined in **Table 6**.

Table 6: Adjusted supply and demand parameters for each scenario.

Scenario	IEEE - 18			IEEE - 30		
	$\%p_{it}^{\omega}$	$\%q_{it}^{\omega}$	$\%n_{\psi t}^{\omega}$	$\%p_{it}^{\omega}$	$\%q_{it}^{\omega}$	$\%n_{\psi t}^{\omega}$
Low	[0.8, 1]	[0.9, 1]	[1, 1.2]	[0.8, 1]	[0.9, 1]	[1, 1.6]
Nominal	1	1	1	1	1	1
High	[1, 1.2]	[1, 1.1]	[0.8, 1]	[1, 1.6]	[1, 1.4]	[0.8, 1]

The low and high scenarios listed in **Table 6** denote the expected demand and supply range that can be sustained within both power networks. The nominal scenario is based on the data retrieved from [49] for each network and is used for benchmarking. The low scenario assumes the demand is reduced while there is an excess supply for a best-case scenario. Conversely, the high scenario assumes supply and demand shocks simultaneously occur for a worst-case scenario. The power quality within the transmission lines throughout these scenarios is illustrated in **Figure 7** for both MGs.

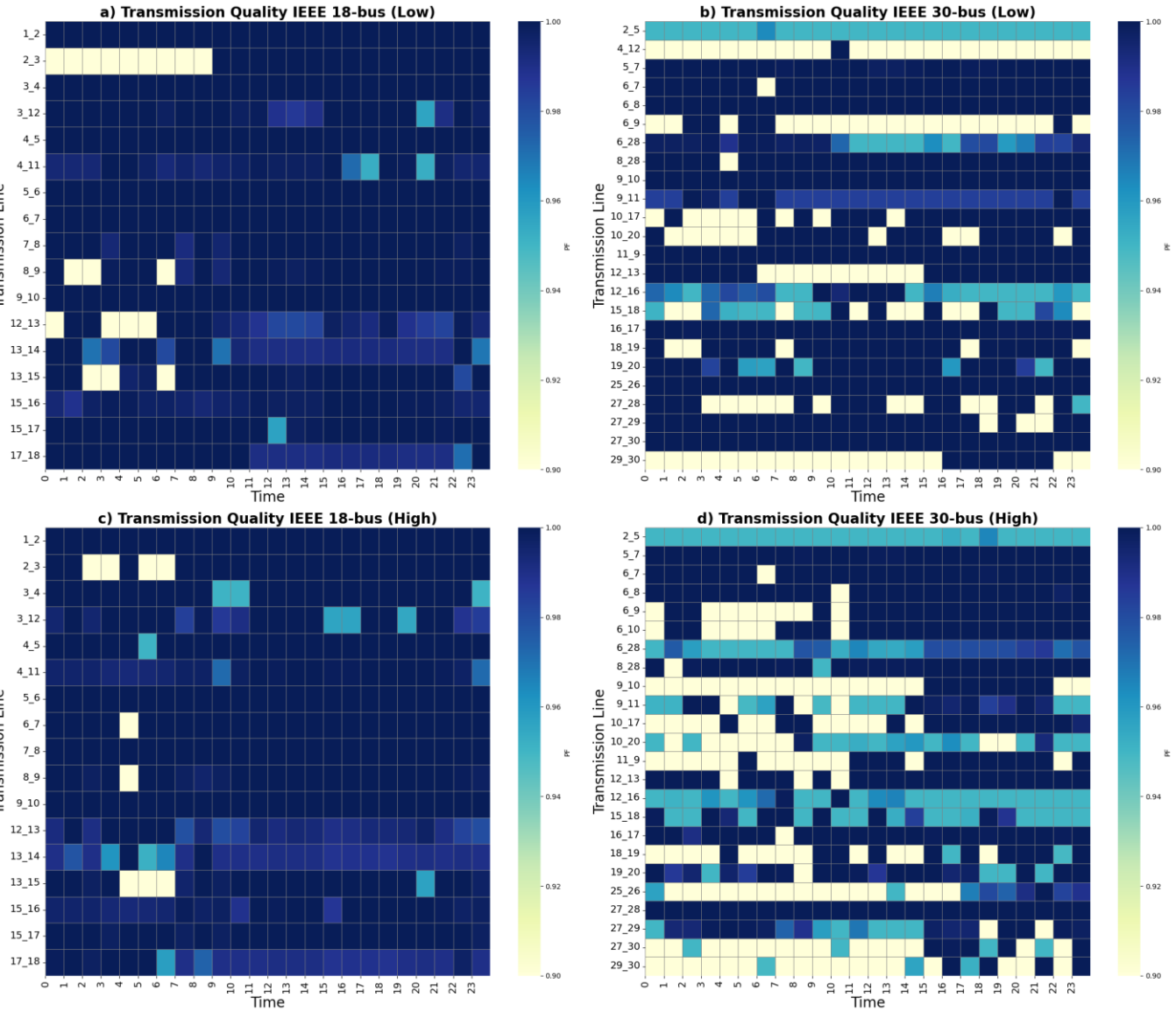

Figure 7: Power quality throughout the transmission lines for the IEEE 18-bus and IEEE 30-bus in both the high and low scenarios

In **Figure 7**, the density of each pixel is calculated using (22) and is proportional to the power quality within the transmission line. The gradient of each pixel allows the TSO to identify poor-performing lines that are either congested or transferring too much reactive power. Lines with zero power flow are not shown in this figure. Since we set PF to 0.95, the periods with white-colored pixels denote PF values less than 0.95. Although white pixels reflect PF values less than the minimum, these PF values may result from low active demand combined with a high reactive supply. This combination is observed in IEEE 18-bus, lines 2_3, 8_9, and 12_3 in **Figure 7a.** The scalability of a transmission line is determined by the ratio of time units that the PF remains above the lower bound to the entire number of time units within the scheduled time horizon. For example, the PF in line 8_9 of **Figure 7a** reaches its lower bound at hours 1,2, and 6. Since

the PF remains above the lower bound for roughly 21/24*100=87.5% of the day, line 8_9 should be considered suitably sized for the expected demand. The performance of these lines slightly improved with additional active demand, as seen in **Figure 7c**. However, **Figure 7b** shows multiple IEEE 30-bus lines that do not sustain the minimum PF for most of the day, including lines 2_5, 4_12, 6_9,15_18, and 29_30. Whereas all IEEE 18-bus lines continue to perform well when additional stress via demand is placed on the MG, as observed in **Figure 8a and 8c,** it is noted to be the opposite case for the IEEE 30-bus system. Except for a few improved lines, **Figures 8b and 8d** show more lines become inefficient for power transmission when additional stress via demand is placed on the MG, including lines 9_10, 10_20, 12_16, 18_19, 25_26, and 27_30. Specifically, lines 2_5 and 4_12 remain above the minimum PF in the low-case scenario for less than 5% of the day, which is unsustainable for long-term transmission network operation. Here, domain knowledge must be stacked onto this analysis since multiple factors influence the PF simultaneously. For example, the IEEE 30-bus system has poor PF but requires no load shedding. Ergo, the poor PF observed may not be due to the IEEE 30-bus transmission capacity but is more likely to result from a high reactive supply throughout the lines. Hence, various mitigation strategies can be employed to improve the PF based on domain knowledge, such as strategically placing inductors through the MG to consume the excess reactive supply.

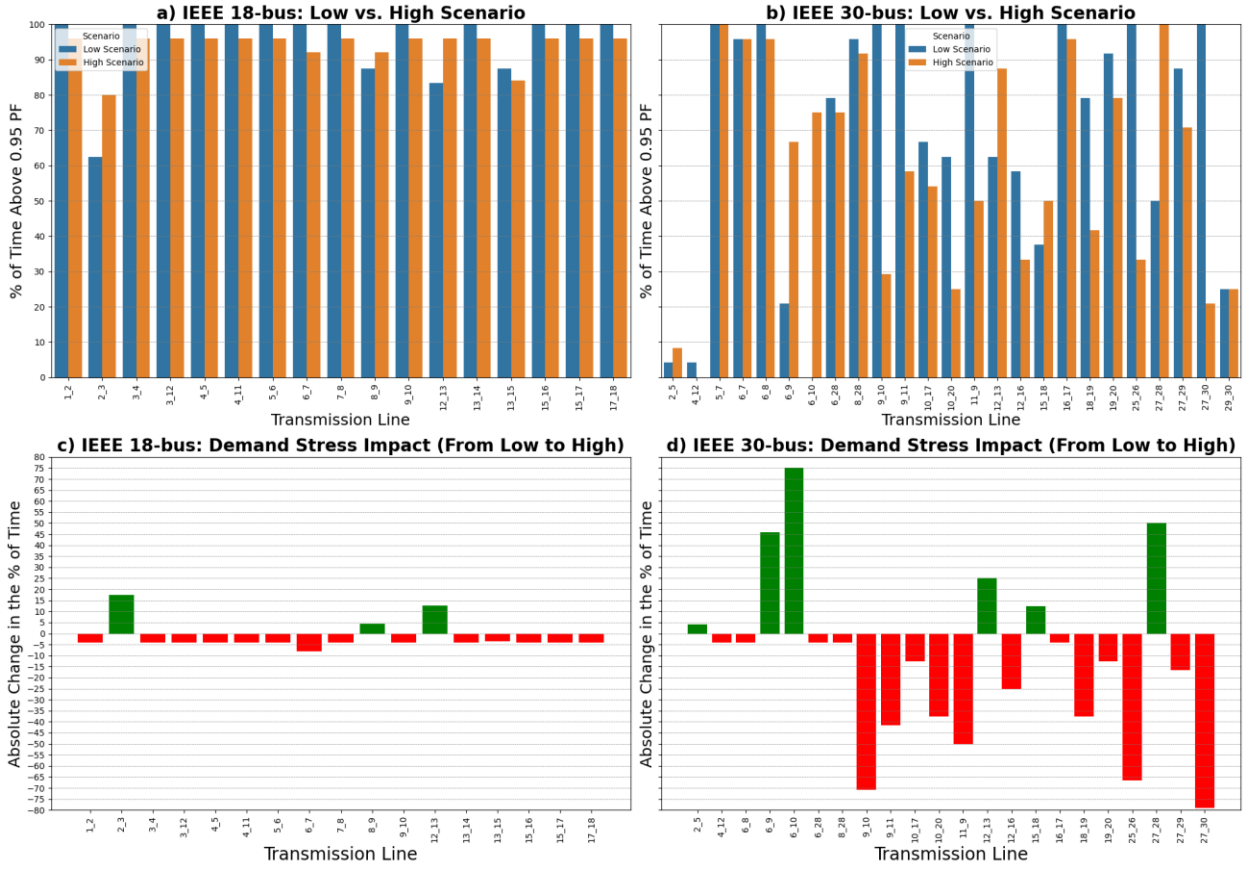

Figure 8: Demand stress impact on power quality of transmission lines for IEEE 18-bus and IEEE 30-bus systems.

3.3 MG Resiliency via Demand & Supply Shocks

After identifying limitations in existing transmission infrastructure while operating at a PF equal to 0.95, we investigate the coordination of the DERs to improve a power network's resiliency to supply and demand

shocks. Based on the power allocations from each class of DERs, the TSO can determine the managerial implications of using the proposed MG dispatch policy. The low and high scenarios listed in **Table 6** were applied to both MGs to observe their change in power allocations from each class of DERs, as shown in **Figure 9**.

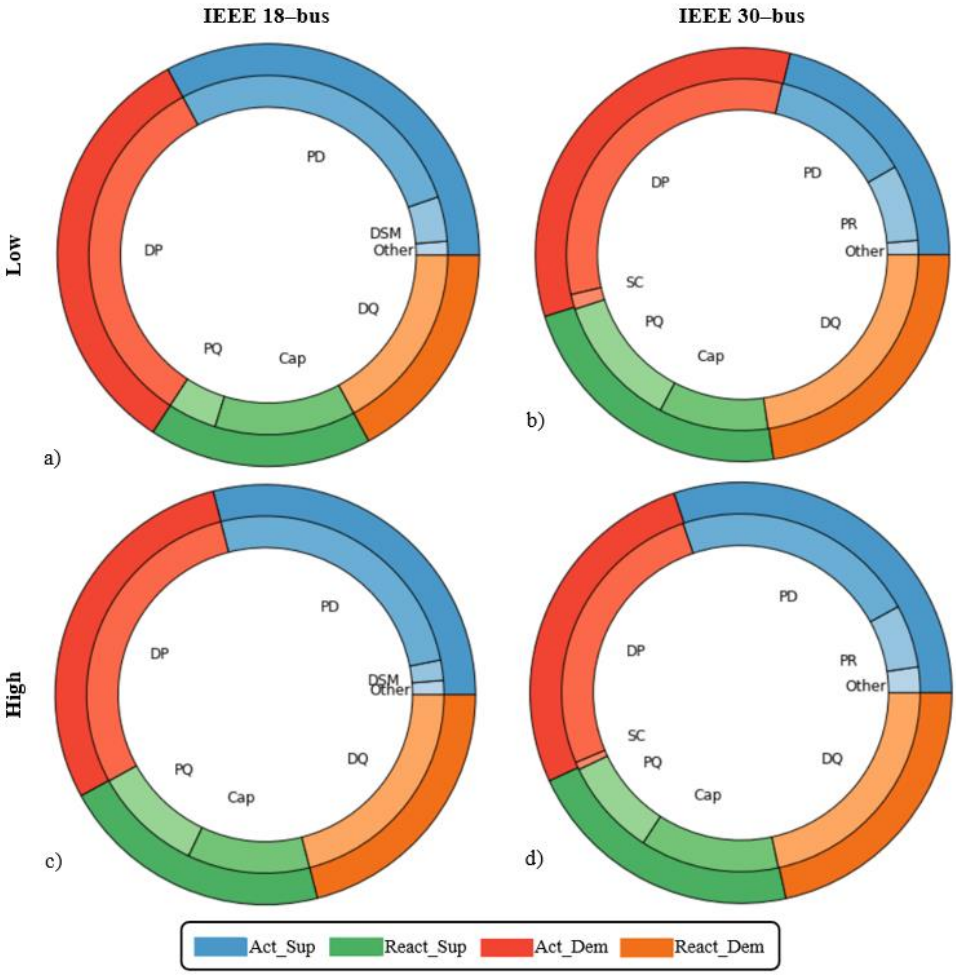

Figure 9: Power allocations from the DERs for the IEEE 18-bus and IEEE 30-bus in both the high and low scenarios

Figure 9 illustrates the active and reactive power portions for each MG supplied by their respective DERs. These two types of power are further decomposed into four major portions based on supply (Act_Sup, React_Sup) and demand (Act_Dem, React_Dem). We note that load shedding via DSM is considered an active supply since it decreases the total active demand. Hence, charging storage units are considered active demand since they decrease the total active supply. If the contribution from a subset of DERs is too small to be visualized, they are grouped as 'Other.' For example, 'Other' in the IEEE 18-bus denotes the active power supplied by the non-dispatchable units, the storage units, and the main utility grid. Similarly, 'Other' in the IEEE 30-bus denotes the active power reduced under the DSM program, supplied by the storage units, and imported from the main utility grid.

During the low scenario, the second largest contribution toward active power was supplied by DSM and the non-dispatchable units in **Figure 9a** and **Figure 9b**, respectively. Thus, the active demand for the IEEE 18-bus is significantly larger than the IEEE 30-bus since load shedding is incurred to "supply" the active

demand that the remaining DERs cannot. The IEEE 18-bus also has a much larger reactive demand than the IEEE 30-bus since its capacitors were near their upper bound in the low scenario. However, during the high scenario, we investigate the re-allocation of power amongst the DERs under demand and supply shocks for each MG. Hence, **Figure 9c** shows that the contribution from the dispatchable units in the IEEE 18-bus increased by 6% and 13% for active and reactive demand, respectively. Although the contributions from DSM and the capacitors seem less significant, they have both nominally increased to meet the supply and demand shocks in the high scenario. Thus, any additional network stress from these shocks is compensated by the dispatchable units in the IEEE 18-bus. However, the IEEE 30-bus has more DERs than the IEEE 18-bus and can better distribute supply and demand shocks. **Figure 9d** shows the contribution from DSM and the capacitors in the IEEE 30-bus increased by 6% and 4% for active and reactive demand, respectively. Both MGs show the same sequence of DER utilization under the proposed MG dispatch policy starting with the non-dispatchable units, then dispatchable units, and finally DSM where necessary. However, the TSO can adjust the priority of DERs by tuning cost parameters to penalize a particular class of DERs where the highest cost is associated with the least desirable supply method.

After prioritizing the supply methods, our proposed MG dispatch policy generates a utilization schedule for the DERs according to a 24-hour planning horizon or day-ahead schedule. A utilization schedule illustrates the optimal generation units within a class of DERs for a given scenario. The utilization schedules for the dispatchable units in both MGs are shown in **Figure 10**.

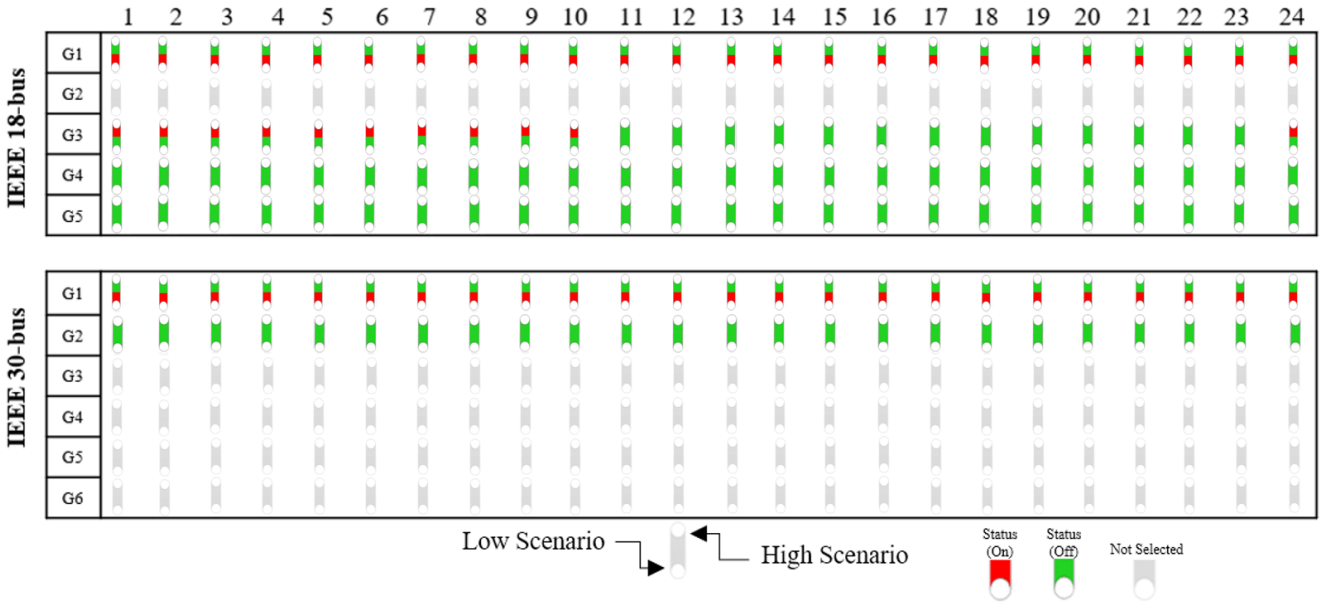

Figure 10: Utilization schedules for the dispatchable units for the IEEE 18-bus and IEEE 30-bus in both the high and low scenarios

In **Figure 10**, the utilization schedule of each dispatchable unit within its respective MG is shown throughout the planning horizon. The state of each dispatchable unit is visually represented by a color indication, with green indicating the unit is on and red indicating it is off for each scenario. The upper and lower indicators compare the use of the dispatchable unit in the low and high scenarios, respectively. During the low scenario, G3 to G5 are selected for the IEEE 18-bus, and G2 is selected for the IEEE 30-bus. However, G1 is added from both MGs during the high scenario to provide additional capacity. Notably, G3

in the IEEE 18-bus was only operational throughout the latter half of the planning horizon (11-24 hours) during the high scenario compared to the entire day during the low scenario. Thus, the cost of operating G1 was less than that of G3 until peak hours, when additional supply was required. If G1 were selected instead of G3 in the low scenario, there would not be sufficient capacity throughout the entire planning horizon; this results in load shedding or the addition of G3. Therefore, utilization schedules help the TSO to identify efficient units within a class of DERs in terms of cost and power quality under the proposed MG dispatch policy. The unselected units in both test networks could not generate power while sustaining a PF equal to 0.95, according to (24). Thus, these units should be replaced with more efficient ones to increase resiliency during a contingency while sustaining the desired power quality in the IEEE 18-bus and IEEE 30-bus.

3.4 Fault Detection & Regulation for MG Stability

The proposed MG dispatch policy utilizes the swing equation in (41) to consider the effect of dispatchable units and contingency reserves on the RF. Under the proposed MG dispatch policy, DSM, poor PF, and large frequency deviations impact the MG's stability compared to a traditional MILP such as [13], which only considers the logistics of power transfer and DSM. Severe faults using a traditional MILP model, which does not consider frequency control, are illustrated in **Figure 9**. Here, the RF and Fnom are calculated to detect and prevent faults within the MG system.

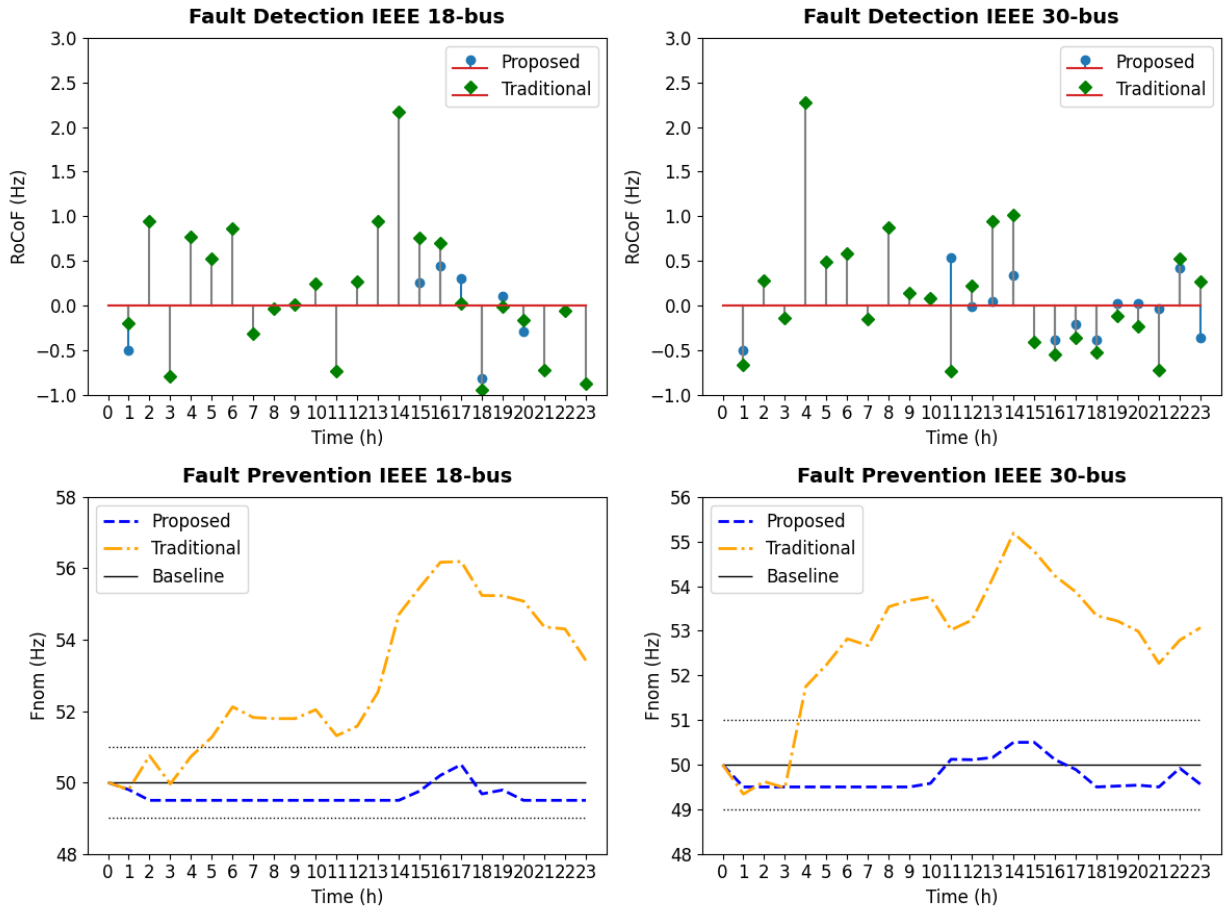

Figure 9. Fault detection and prevention for the IEEE 18-bus and IEEE 30-bus

In **Figure 11**, the RF and Fnom curves must remain within their operating limits to prevent a fault from cascading by tripping protection relays. Please note that **Figure 11** shows the effect of an impulse in

frequency at each hour, not the time it takes to reach equilibrium, which is on a second timescale. In **Figure 11**, faults occur more frequently in the IEEE 18-bus under the traditional model, with violations at hours 2, 14, and 18. However, faults occur roughly 70% less under the proposed MG dispatch policy and remain within the tolerance region specified by the TSO. The proposed MG dispatch policy arrests the post-fault RF and subsequently limits the deviation of the Fnom. The Fnom curve reflects the consequent deviations in the nominal frequency incurred due to the deviations in the RF, where deviations in Fnom persist until another fault occurs. Specifically, significant frequency fluctuations occur between hours 18 and 20 in the IEEE 18-bus, which synchronizes with peak demand. The market-clearing price of energy is volatile during peak demand, and DSM is often required to maintain stability during supply and demand shocks. Thus, the Fnom deviates significantly from the baseline operating frequency under the traditional model compared to the proposed MG dispatch policy. A similar behavior for the RF and Fnom was observed for the IEEE 30-bus, as shown in **Figure 11**. Since the Fnom of the MG is permanently affected at these hours, restorative measures are taken to stabilize the MG. These restorative measures follow the same sequence of DER utilization (see Section 3.3) starting with the non-dispatchable units, then dispatchable units, and finally DSM where necessary. Under the proposed MG dispatch policy, the MG system is fault-tolerant and will remain stable to prevent network collapse while sustaining the minimal cost and CO_2 emissions required to operate.

4 CONCLUSION

This study proposes an ODD framework that employs a novel MG dispatch policy to minimize the total operational cost while considering power flow physics, the mechanical limitations of each DER, and the influence of economic and climate factors on power transfer. In addition, a rolling horizon heuristic is introduced to obtain solutions faster on average by dividing the original problem into smaller sub-problems that are solved sequentially. The best-compromise solution between the conflicting objectives of cost and emissions showed that prioritizing emissions significantly reduced emissions but slightly increased operational cost in both the IEEE 18-bus and the IEEE 30-bus systems. The power quality of the IEEE 18-bus was improved since our MG dispatch policy disproportionally reduces reactive demand during load shedding. Setting the PF to 0.95 in the IEEE 18-bus system resulted in a 10% and 60% reduction in the active and reactive demand, respectively.

Moreover, no load shedding was observed in the IEEE 30-bus system at a PF of 0.95, and faults remained within their respective tolerance region for both MGs. The proposed MG dispatch policy is effective for identifying and replacing/resizing poor performing DERs and transmission lines with low PF. The sequence of power supplied by the DERs to address a contingency under the proposed MG dispatch policy starts with non-dispatchable units, then dispatchable units, and finally, DSM where necessary. Although this sequence can be adjusted, it is currently the ideal sequence to prioritize clean energy. In future work, shiftable and dimmable loads could be considered in the proposed DSM program to enhance MG operational efficiency at the appliance level as cities transition toward a smart grid architecture.

CRediT AUTHORSHIP CONTRIBUTION STATEMENT

Abdullah Alsaheal: Investigation, Validation, Visualization, Data curation, Writing – review & editing. **Joshua Darville:** Conceptualization, Methodology, Software, Data curation, Writing – original draft. **Haluk Damgacioglu:** Conceptualization, Methodology, Writing – review & editing. **Nurcin Celik:** Conceptualization, Methodology, Writing – review & editing, Supervision. **Murat Erkoc:** Conceptualization, Methodology, Writing – review & editing.

DECLARATION OF COMPETING INTEREST

The authors declare that they have no known competing financial interests or personal relationships that could have appeared to influence the work reported in this paper.

ACKNOWLEDGMENT

This work was supported in part by the AFOSR Award No: FA9550-18-1-0075.

REFERENCES

[1] D. K. Panda and S. Das, "Smart grid architecture model for control, optimization and data analytics of future power networks with more renewable energy," *J Clean Prod*, vol. 301, p. 126877, Jun. 2021, doi: 10.1016/J.JCLEPRO.2021.126877.

[2] M. A. O. Schroeder, M. T. C. de Barros, A. C. S. Lima, M. M. Afonso, and R. A. R. Moura, "Evaluation of the impact of different frequency dependent soil models on lightning overvoltages," *Electric Power Systems Research*, vol. 159, pp. 40–49, Jun. 2018, doi: 10.1016/J.EPSR.2017.09.020.

[3] J. Darville and N. Celik, "Microgrid Operational Planning Using Deviation Clustering Within a DDDAS Framework," in *International Conference on Dynamic Data Driven Application Systems*, 2020, pp. 77–84. doi: doi.org/10.1007/978-3-030-61725-7_11.

[4] J. Darville and C. Nurcin, "Simulation Optimization for Unit Commitment using a Region-based Sampling (RBS) Algorithm," in *Proceedings of the 2020 IISE Annual Conference*, 2020.

[5] S. Ullah, A. M. A. Haidar, P. Hoole, H. Zen, and T. Ahfock, "The current state of Distributed Renewable Generation, challenges of interconnection and opportunities for energy conversion based DC microgrids," *J Clean Prod*, vol. 273, p. 122777, Nov. 2020, doi: 10.1016/J.JCLEPRO.2020.122777.

[6] B. Mukhopadhyay and D. Das, "Optimal multi-objective long-term sizing of distributed energy resources and hourly power scheduling in a grid-tied microgrid," *Journal Pre-proof*, 2022, doi: 10.1016/j.segan.2022.100632.

[7] J. D. Rios Penaloza, J. A. Adu, A. Borghetti, F. Napolitano, F. Tossani, and C. A. Nucci, "Influence of load dynamic response on the stability of microgrids during islanding transition," *Electric Power Systems Research*, vol. 190, Jan. 2021, doi: 10.1016/j.epsr.2020.106607.

[8] H. Chen, L. Zhang, Q. Liu, H. Wang, and X. Dai, "Simulation-based vulnerability assessment in transit systems with cascade failures," *J Clean Prod*, vol. 295, p. 126441, May 2021, doi: 10.1016/J.JCLEPRO.2021.126441.

[9] W. J. Wright, J. Darville, N. Celik, H. Koerner, and E. Celik, "In-situ optimization of thermoset composite additive manufacturing via deep learning and computer vision," *Addit Manuf*, vol. 58, p. 102985, Oct. 2022, doi: 10.1016/j.addma.2022.102985.

[10] C. D. Philippe, W. M. Hamilton, A. C. Penn, and J. M. Shultz, "Innovative health professional leadership for a climate-resilient Bahamas," *The Journal of Climate Change and Health*, vol. 4, p. 100055, Oct. 2021, doi: 10.1016/J.JOCLIM.2021.100055.

[11] M. Mehdi, S. Z. Jamali, M. O. Khan, S. Baloch, and C. H. Kim, “Robust control of a DC microgrid under parametric uncertainty and disturbances,” *Electric Power Systems Research*, vol. 179, p. 106074, Feb. 2020, doi: 10.1016/J.EPSR.2019.106074.

[12] X. Shi, H. Damgacioglu, and N. Celik, “A dynamic data-driven approach for operation planning of microgrids,” *Procedia Comput Sci*, vol. 51, no. 1, pp. 2543–2552, 2015, doi: 10.1016/j.procs.2015.05.362.

[13] H. Damgacioglu, M. Bastani, and N. Celik, “A Dynamic Data-Driven Optimization Framework for Demand Side Management in Microgrids,” *Handbook of Dynamic Data Driven Applications Systems*, pp. 489–504, 2018, doi: 10.1007/978-3-319-95504-9_21.

[14] S. M. Nosratabadi, R. A. Hooshmand, E. Gholipour, and S. Rahimi, “Modeling and simulation of long term stochastic assessment in industrial microgrids proficiency considering renewable resources and load growth,” *Simul Model Pract Theory*, vol. 75, pp. 77–95, Jun. 2017, doi: 10.1016/J.SIMPAT.2017.03.013.

[15] A. Nasri, S. J. Kazempour, A. J. Conejo, and M. Ghandhari, “Network-constrained AC unit commitment under uncertainty: A benders’ decomposition approach,” *IEEE Transactions on Power Systems*, vol. 31, no. 1, pp. 412–422, 2016, doi: 10.1109/TPWRS.2015.2409198.

[16] M. E. Baran and F. F. Wu, “Network reconfiguration in distribution systems for loss reduction and load balancing,” *IEEE transactions on power delivery*, vol. 4, no. 2, pp. 1401–1407, 1989, doi: 10.1109/61.25627.

[17] H. Damgacioglu and N. Celik, “A two-stage decomposition method for integrated optimization of islanded AC grid operation scheduling and network reconfiguration,” *International Journal of Electrical Power & Energy Systems*, vol. 136, p. 107647, Mar. 2022, doi: 10.1016/J.IJEPES.2021.107647.

[18] A. Yavuz *et al.*, “Advancing Self-Healing Capabilities in Interconnected Microgrids via DDDAS with Relational Database Management,” in *Proceedings of the 2020 Winter Simulation Conference*, 2020. [Online]. Available: https://informs-sim.org/wsc20papers/214.pdf

[19] A. E. Thanos, M. Bastani, N. Celik, and C. Chen, “Framework for Automated Control in Microgrids,” *IEEE Trans Smart Grid*, vol. 8, no. 1, pp. 209–218, 2017.

[20] G. Mavrotas, “Effective implementation of the ε-constraint method in Multi-Objective Mathematical Programming problems,” *Appl Math Comput*, vol. 213, no. 2, pp. 455–465, 2009, doi: 10.1016/j.amc.2009.03.037.

[21] M. Bastani, H. Damgacioglu, and N. Celik, “A δ-constraint multi-objective optimization framework for operation planning of smart grids,” *Sustain Cities Soc*, vol. 38, no. November 2017, pp. 21–30, 2018, doi: 10.1016/j.scs.2017.12.006.

[22] H. Mortaji, S. H. Ow, M. Moghavvemi, and H. A. F. Almurib, “Load Shedding and Smart-Direct Load Control Using Internet of Things in Smart Grid Demand Response Management,” *IEEE Trans Ind Appl*, vol. 53, no. 6, pp. 5155–5163, 2017, doi: 10.1109/TIA.2017.2740832.

[23] P. A. Giglou and S. Najafi Ravadanegh, “Defending against false data injection attack on demand response program: A bi-level strategy,” *Sustainable Energy, Grids and Networks*, vol. 27, p. 100506, Sep. 2021, doi: 10.1016/J.SEGAN.2021.100506.

[24] A. Bolurian, H. Akbari, and S. Mousavi, “Day-ahead optimal scheduling of microgrid with considering demand side management under uncertainty,” Electric Power Systems Research, vol. 209, p. 107965, 2022. doi:10.1016/j.epsr.2022.107965

[25] Y. Wen, W. Li, G. Huang, and X. Liu, “Frequency Dynamics Constrained Unit Commitment with Battery Energy Storage,” *IEEE Transactions on Power Systems*, vol. 31, no. 6, pp. 5115–5125, 2016, doi: 10.1109/TPWRS.2016.2521882.

[26] Y. Wen, C. Y. Chung, X. Liu, and L. Che, “Microgrid dispatch with frequency-aware islanding constraints,” *IEEE Transactions on Power Systems*, vol. 34, no. 3, pp. 2465–2468, May 2019, doi: 10.1109/TPWRS.2019.2895573.

[27] Y. Tofis, S. Timotheou, and E. Kyriakides, “Minimal Load Shedding Using the Swing Equation,” *IEEE Transactions on Power Systems*, vol. 32, no. 3, pp. 2466–2467, 2017, doi: 10.1109/TPWRS.2016.2614886.

[28] M. M. Islam, X. Zhong, Z. Sun, H. Xiong, and W. Hu, “Real-time frequency regulation using aggregated electric vehicles in smart grid,” *Comput Ind Eng*, vol. 134, 2019, doi: 10.1016/j.cie.2019.05.025.

[29] S. Shojaei, J. Beiza, T. Abedinzadeh, and H. Alipour, "Optimal eco-emission scheduling of a microgrid by considering uncertainties," Journal of Energy Management and Technology, vol. 6, no. 2, pp. 119-126, 2022. DOI: 10.22109/jemt.2021.289829.1306.

[30] Y. R. Rodrigues, W. Eberle, M. S. Metcalfe, and A. C. Z. Souza, “Impact of appliances harmonic content in microgrid environments,” *2015 IEEE PES Innovative Smart Grid Technologies Latin America, ISGT LATAM 2015*, pp. 701–705, 2016, doi: 10.1109/ISGT-LA.2015.7381242.

[31] F. A. Rahiman, H. H. Zeineldin, V. Khadkikar, S. W. Kennedy, and V. R. Pandi, “Demand Response Mismatch (DRM): Concept, Impact Analysis, and Solution,” *IEEE Trans Smart Grid*, vol. 5, pp. 1734–1743, 2014, doi: 10.1109/TSG.2014.2309995.

[32] G. M. Kopanos and E. N. Pistikopoulos, “Reactive scheduling by a multiparametric programming rolling horizon framework: A case of a network of combined heat and power units,” *Ind Eng Chem Res*, vol. 53, no. 11, pp. 4366–4386, 2014, doi: 10.1021/ie402393s.

[33] J. Silvente, G. M. Kopanos, V. Dua, and L. G. Papageorgiou, “A rolling horizon approach for optimal management of microgrids under stochastic uncertainty,” *Chemical Engineering Research and Design*, vol. 131, pp. 293–317, 2018, doi: 10.1016/j.cherd.2017.09.013.

[34] F. Kamal and B. Chowdhury, “Model predictive control and optimization of networked microgrids,” *International Journal of Electrical Power & Energy Systems*, vol. 138, p. 107804, Jun. 2022, doi: 10.1016/J.IJEPES.2021.107804.

[35] V. Sarfi and H. Livani, “An economic-reliability security-constrained optimal dispatch for microgrids,” *IEEE Transactions on Power Systems*, vol. 33, no. 6, pp. 6777–6786, 2018, doi: 10.1109/TPWRS.2018.2835421.

[36] R. Bajool, M. Shafie-Khah, A. S. Gazafroudi, and J. P. S. Catalao, “Mitigation of active and reactive demand response mismatches through reactive power control considering static load modeling in distribution grids,” *1st Annual IEEE Conference on Control Technology and Applications, CCTA 2017*, vol. 2017-Janua, pp. 1637–1642, 2017, doi: 10.1109/CCTA.2017.8062691.

[37] W. B. Powell and S. Meisel, “Tutorial on Stochastic Optimization in Energy—Part I: Modeling and Policies,” *IEEE Transactions on Power Systems*, vol. 31, no. 2, pp. 1459–1467, 2016, doi: 10.1109/TPWRS.2015.2424980.

[38] W. B. Powell and S. Meisel, “Tutorial on Stochastic Optimization in Energy - Part II: An Energy Storage Illustration,” *IEEE Transactions on Power Systems*, vol. 31, no. 2, pp. 1468–1475, 2016, doi: 10.1109/TPWRS.2015.2424980.

[39] L. A. Hannah, “Stochastic Optimization,” *Encyclopedia of Actuarial Science*, pp. 1–20, 2004, doi: 10.1002/9780470012505.tas034.

[40] S. F. Al-Gahtani and R. M. Nelms, “A frequency adaptive control scheme for a three-phase shunt active power filter,” *Electrical Engineering*, vol. 103, no. 1, pp. 595–606, Feb. 2021, doi: 10.1007/s00202-020-01105-4.

[41] S. F. Al-Gahtani, H. Z. Azazi, R. M. Nelms, and Z. M. Elbarbary, “Detection of negative sequence components in diagnosing and tolerating open-gate fault for a voltage-source inverter in an induction motor drive,” *IET Power Electronics*, vol. 13, no. 18, pp. 4194–4203, Dec. 2020, doi: 10.1049/iet-pel.2020.0289.

[42] A. Dadashzade, F. Aminifar and M. Davarpanah, "Unbalanced Source Detection in Power Distribution Networks by Negative Sequence Apparent Powers," in IEEE Transactions on Power Delivery, vol. 36, no. 1, pp. 481-483, Feb. 2021, doi: 10.1109/TPWRD.2020.3029437.

[43] J. Darville, J. Curia, and N. Celik, “Microgrid Operational Planning using a Hybrid Neural Network with Resource-aware Scenario Selection,” *Simul Model Pract Theory*, vol. 119, p. 102583, Sep. 2022, doi: 10.1016/j.simpat.2022.102583.

[44] M. E. Baran and F. F. Wu, “Network reconfiguration in distribution systems for loss reduction and load balancing,” *IEEE Transactions on Power Delivery*, vol. 4, no. 2, pp. 1401–1407, 1989, doi: 10.1109/61.25627.

[45] S. Chalil Madathil *et al.*, “Resilient off-grid microgrids: Capacity planning and N-1 security,” *IEEE Trans Smart Grid*, vol. 9, no. 6, pp. 6511–6521, Nov. 2018, doi: 10.1109/TSG.2017.2715074.

[46] L. Gan, N. Li, U. Topcu, and S. H. Low, “Exact Convex Relaxation of Optimal Power Flow in Radial Networks,” *IEEE Trans Automat Contr*, vol. 60, no. 1, pp. 72–87, 2015, doi: 10.1109/TAC.2014.2332712.

[47] J. Hartleb and M. Schmidt, “A rolling horizon heuristic with optimality guarantee for an on-demand vehicle scheduling problem,” *OpenAccess Series in Informatics*, vol. 85, no. 15, pp. 1–15, 2020, doi: 10.4230/OASIcs.ATMOS.2020.15.

[48] A. Setämaa-Kärkkäinen, K. Miettinen, and J. Vuori, “Best compromise solution for a new multiobjective scheduling problem,” *Comput Oper Res*, vol. 33, no. 8, pp. 2353–2368, 2006, doi: 10.1016/j.cor.2005.02.006.

[49] R. D. Zimmerman, C. E. Murillo-Sánchez, and R. J. Thomas, “MATPOWER: Steady-state operations, planning, and analysis tools for power systems research and education,” *IEEE Transactions on Power Systems*, vol. 26, no. 1, pp. 12–19, Feb. 2011, doi: 10.1109/TPWRS.2010.2051168.

[50] “IEEE 30-bus data.” http://labs.ece.uw.edu/pstca/pf30/pg_tca30bus.htm (accessed Apr. 11, 2022).

[51] Energy Star Program, “Energy Star Program Requirements for Single Voltage External AC-DC and AC-AC power supplies - Eligibility Criteria (Version 2.0),” 2008.

DECLARATION OF COMPETING INTEREST

The authors declare that they have no known competing financial interests or personal relationships that could have appeared to influence the work reported in this paper.

Nurcin Celik on behalf of the authors: _____